MOZART1 and γ-tubulin complex receptors are both required to turn γ-TuSC into an active microtubule nucleation template

Tien-chen Lin,[1] Annett Neuner,[1] Dirk Flemming,[2] Peng Liu,[1] Takumi Chinen,[1] Ursula Jäkle,[1] Robert Arkowitz,[3] and Elmar Schiebel[1]

[1]Zentrum für Molekulare Biologie der Universität Heidelberg, DKFZ-ZMBH-Allianz, 69120 Heidelberg, Germany
[2]Biochemistry Center, 69120 Heidelberg, Germany
[3]Université Côte d'Azur, Centre National de la Recherche Scientifique, Institut National de la Santé et de la Recherche Médicale, Institut de Biologie Valrose, 06108 Nice, France

MOZART1/Mzt1 is required for the localization of γ-tubulin complexes to microtubule (MT)–organizing centers from yeast to human cells. Nevertheless, the molecular function of MOZART1/Mzt1 is largely unknown. Taking advantage of the minimal MT nucleation system of *Candida albicans*, we reconstituted the interactions of Mzt1, γ-tubulin small complex (γ-TuSC), and γ-tubulin complex receptors (γ-TuCRs) Spc72 and Spc110 in vitro. With affinity measurements, domain deletion, and swapping, we show that Spc110 and Mzt1 bind to distinct regions of the γ-TuSC. In contrast, both Mzt1 and γ-TuSC interact with the conserved CM1 motif of Spc110/Spc72. Spc110/Spc72 and Mzt1 constitute "oligomerization chaperones," cooperatively promoting and directing γ-TuSC oligomerization into MT nucleation-competent rings. Consistent with the functions of Mzt1, human MOZART1 directly interacts with the CM1-containing region of the γ-TuCR CEP215. MOZART1 depletion in human cells destabilizes the large γ-tubulin ring complex and abolishes CEP215^{CM1}-induced ectopic MT nucleation. Together, we reveal conserved functions of MOZART1/Mzt1 through interactions with γ-tubulin complex subunits and γ-TuCRs.

Introduction

The microtubule (MT) nucleating activity at MT-organizing centers (MTOCs), such as the mammalian centrosome or the yeast spindle pole body (SPB), primarily depends on γ-tubulin. γ-Tubulin is a member of the tubulin superfamily alongside α- and β-tubulin. γ-Tubulin combines with GCP2 and GCP3 to form the tetrameric γ-tubulin small complex (γ-TuSC) that contains γ-tubulin, GCP2, and GCP3 in a 2:1:1 ratio (Knop and Schiebel, 1997). γ-TuSC is best characterized in *Saccharomyces cerevisiae*. The purified *S. cerevisiae* γ-TuSC (Scγ-TuSC) composed of Tub4 (γ-tubulin), Spc97 (GCP2), and Spc98 (GCP3) has a Y- or V-shape conformation (Kollman et al., 2008). γ-TuSC is able to oligomerize into a 13-fold symmetric spiral-like structure in vitro upon binding to the N-terminal fragment of Spc110 (Spc110-N), the γ-tubulin complex receptor (γ-TuCR) that recruits γ-TuSC to the nuclear side of the SPB (Knop and Schiebel, 1998; Kollman et al., 2010). The diameter and the pitch of the γ-TuSC–Spc110-N rings resemble those of the MT cylinder, suggesting that the oligomerized γ-TuSC functions as a MT nucleation template (Kollman et al., 2010). Although Spc110 has this γ-TuSC oligomerization function at the nuclear side of the SPB, this role is likely fulfilled by the γ-TuCR Spc72 at the SPB cytoplasmic side (Knop and Schiebel, 1998).

γ-TuSC components are highly conserved and essential for viability in all eukaryotes (Knop and Schiebel, 1997; Martin et al., 1998; Tange et al., 2004; Colombié et al., 2006; Liu and Lessman, 2007; Seltzer et al., 2007; Nakamura and Hashimoto, 2009; Xiong and Oakley, 2009). However, in many organisms such as *Schizosaccharomyces pombe*, *Drosophila melanogaster*, and human cells, the γ-TuSC assembles with additional subunits into the stable, 2.2-MD large γ-tubulin ring complex (γ-TuRC; Gunawardane et al., 2000; Zhang et al., 2000; Murphy et al., 2001; Anders et al., 2006). The γ-TuRC comprises multiple copies of γ-TuSC together with substochiometric levels of the GCP proteins GCP4, GCP5, and GCP6 (Choi et al., 2010). These GCP proteins as well as GCP2 and GCP3 share two conserved structures, the GRIP1 and GRIP2 domains (Gunawardane et al., 2000). However, GCP4–6 are missing from the fungal species of subphylum Saccharomycotina, including the budding yeast *S. cerevisiae* (Lin et al., 2015).

Correspondence to Elmar Schiebel: schiebel.elmar@zmbh.uni-heidelberg.de

Abbreviations used: Caγ-TuSC, *Candida albicans* γ-tubulin small complex; CBB, Coomassie brilliant blue; Dox, doxycycline; γ-TuCR, γ-tubulin complex receptor; γ-TuRC, γ-tubulin ring complex; γ-TuSC, γ-tubulin small complex; MST, microscale thermophoresis; MT, microtubule; MTOC, microtubule-organizing center; NSC, nonspecific control; Scγ-TuSC, *Saccharomyces cerevisiae* γ-tubulin small complex; SPB, spindle pole body; SPM, Spc110/Pcp1 motif.

The Rockefeller University Press $30.00
J. Cell Biol. Vol. 215 No. 6 823–840
https://doi.org/10.1083/jcb.201606092

MOZART1/Mzt1 is highly conserved in most eukaryotes with the exception of *S. cerevisiae*, which completely lacks an *MZT1* gene. It was first identified in a systematic tandem-affinity purification screen for human proteins required in mitosis (Hutchins et al., 2010; Teixidó-Travesa et al., 2010). Human cells encode two MOZART paralogues, MOZART1 and MOZART2A/2B. Although RNAi knockdown of MOZART2A/B only mildly reduced the recruitment of γ-TuRC to interphase centrosomes and did not invoke mitotic defects (Teixidó-Travesa et al., 2010), knockdown of the human MOZART1 reduced binding of γ-TuRC to mitotic centrosomes, leading to the generation of monopolar mitotic spindles (Hutchins et al., 2010). Little is known about the molecular function of MOZART1/Mzt1 beyond the facts that the MOZART1/Mzt1 proteins of *S. pombe* and *Arabidopsis thaliana* interact with the N terminus of GCP3 in the yeast two-hybrid system and that the *S. pombe MZT1* gene somehow cooperates with GCP6 in recruiting γ-TuSC to the SPB (Janski et al., 2012; Dhani et al., 2013; Masuda and Toda, 2016). Presently, it is unclear whether MOZART1/Mzt1 acts solely as a γ-TuSC recruiting factor or whether it can also support γ-TuCRs such as Spc110 in facilitating γ-TuSC oligomerization. It is also unclear why *MZT1* is absent from *S. cerevisiae,* yet essential for MT nucleation and viability in all other tested model organisms (human cells, *A. thaliana*, and *S. pombe*). Moreover, it remains to be determined whether the functions of fungal Mzt1 are conserved or diverged in human cells.

Candida albicans is a diploid fungus that grows as both ovoid budding yeast and filamentous hyphae. *C. albicans* is able to form true hyphae when grown in a medium that mimics the physiological environment of the human host (Mackenzie, 1962). The ability to form hyphae enables this opportunistic fungal pathogen to invade tissues and provoke systemic infections in immunocompromised patients. The set of proteins for MT nucleation are identical in *C. albicans* and *S. cerevisiae* (γ-TuSC and γ-TuCRs), except that *MZT1* is only encoded by *C. albicans*.

To understand the function of Mzt1 in a γ-TuSC–only organism, we reconstituted the *C. albicans* MT nucleation system in vitro with purified components. Mechanistically, we revealed that CaMzt1 bound directly to both *C. albicans* γ-TuSC (Caγ-TuSC) and the γ-TuCRs featuring the CaSpc98-N and the conserved CM1 region, respectively (Samejima et al., 2008; Lin et al., 2014). CaMzt1 cooperated with γ-TuCRs in inducing compact, MT nucleation-competent Caγ-TuSC rings. Consistent with a conserved role in promoting γ-TuSC oligomerization for CaMzt1, RNAi knockdown of MOZART1 in U2OS cells led to the accumulation of the γ-TuSC and a decline in γ-TuRC levels. Moreover, MOZART1 showed high-affinity interaction with the human γ-TuCR CEP215 (also known as CDK5RAP2) that interacts with the γ-TuRC and stimulates MT nucleation activity (Choi et al., 2010). In summary, we reveal an unexpectedly pivotal role for the small protein MOZART1/Mzt1 in regulating γ-tubulin ring assembly and MT nucleation.

Results

CaMzt1 is required for the targeting of γ-TuSC to SPBs and mitotic spindle assembly

To determine whether the presence of *MZT1* is correlated with the presence of *GCP4–6*, we searched the genomes of the fungal species of Saccharomycotina, which lack *GCP4–6*, for homologues of *MZT1*. We found that species within the CTG clade of the Saccharomycotina encode a putative *MZT1* gene, despite the absence of *GCP4–6* (Fig. S1 A and Table S1). The CTG-clade Mzt1 homologues share high similarity with MOZART1/Mzt1 proteins from *S. pombe*, Arabidopsis, and human cells (Fig. S1 B).

We selected *C. albicans* (SC5314) to study the function of Mzt1 because the methods for genetic manipulation are well established, and the organism is an opportunistic pathogen. We first asked whether *MZT1* is essential for viability in *C. albicans*. We were able to disrupt one of the two *MZT1* copies of the diploid *C. albicans* (Fig. S1 C, *mzt1Δ::URA3/MZT1*). However, using this same deletion cassette, we were unable to disrupt the second *MZT1* copy in *mzt1Δ::NAT/MZT1* cells, as all Ura^+ colonies were *mzt1Δ::NAT/MZT1* (Fig. S1 C). These data suggest that *MZT1* is most likely an essential gene in *C. albicans*.

To study the CaMzt1 functions in vivo, we constructed *C. albicans* cells in which one copy of *MZT1* was deleted, and the remaining copy was placed under the control of the Tet_{off} promoter (Δ/Tetp-*CaMZT1*). To detect depletion of CaMzt1 and visualize the localization of CaMzt1, GFP was fused to Tetp-*MZT1* (Tetp-*MZT1-GFP*). In the absence of a functional repressor (no doxycycline [−Dox]), CaMzt1-GFP appeared as one or two dotlike signals at the nuclear periphery, which were most likely at SPBs, throughout the cell cycle (Fig. 1 A). Dox addition strongly reduced the dotlike CaMzt1-GFP signals at spindle poles of Δ/Tetp-*CaMZT1-GFP* cells (Fig. 1 A, +Dox). In contrast, the CaMzt1-GFP SPB localization of *CaMZT1-GFP/MZT1* cells that expressed *CaMZT1-GFP* from the endogenous promoter was unaffected by Dox (Fig. S1 D). To visualize Caγ-TuSC localization, *CaSPC97* or *CaSPC98* was tagged with GFP in Δ/Tetp-*CaMZT1* cells. Upon Dox repression of *CaMZT1*, the intensity of the punctuate SPB signal of CaSpc97-GFP and CaSpc98-GFP was reduced (Fig. 1 B and Fig. S1 E), suggesting that localization of Caγ-TuSC components with the SPB is dependent on CaMzt1.

Live-cell imaging was performed to understand the role of CaMzt1 in MT organization. In contrast to the relative constant number of MTs at SPBs in *S. cerevisiae* (Winey et al., 1995), MTs at SPBs of *C. albicans* increased with the onset of budding (Fig. S1 F, +CaMzt1; and Video 1, cell 1: −5 to 0 min; cell 2: −10 to 0 min), consistent with data from fixed cells (Barton and Gull, 1988). Different from *S. cerevisiae*, SPB-detached MTs were present in *C. albicans* (Fig. 1 C, enlargement, arrows; and Fig. S1 F, enlargement; Barton and Gull, 1988; Finley and Berman, 2005). These free MTs were abundant during early interphase and diminished at the onset of mitotic spindle assembly (Video 1). The free MTs probably derived from SPB-detached MTs or MT fragmentation during spindle disassembly with mitotic exit (Fig. 1 C, +CaMzt1).

Upon Dox treatment to suppress *CaMZT1* expression, nearly all of the cells had defects in mitotic spindle assembly during the 120-min observation window, although the daughter cells grew into a large bud, indicating that cell growth was unaffected (Fig. 1 C, −CaMzt1; Fig. S1 F, −CaMzt1; and Video 2). About 85% of cells only had a single dotlike MT signal, likely representing unseparated SPBs caused by an MT nucleation defect (Fig. 1, C [−CaMzt1] and D; and Video 2, cell 1). Although in the residual 15% of cells, short mitotic spindles were formed (Fig. 1 D, −CaMzt1), spindles either collapsed shortly after they were established

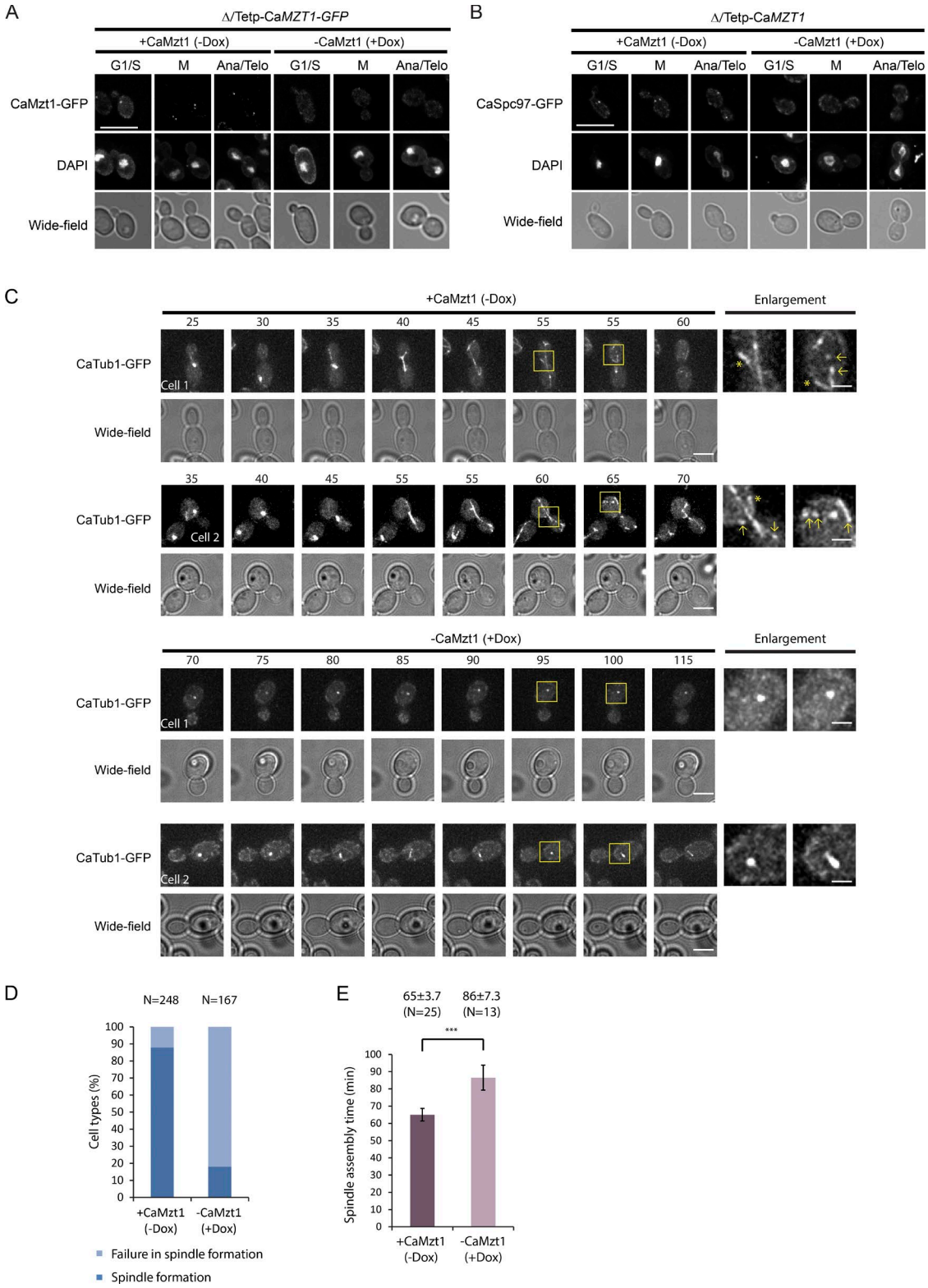

Figure 1. **Depletion of *MZT1* in *C. albicans* delocalizes Caγ-TuSC from SPBs and disrupts MT organization.** (A) CaMzt1-GFP associates with SPBs throughout the cell cycle. Δ/Tetp-*CaMZT1-GFP* cells were grown with and without Dox to control *CaMZT1-GFP* expression. DNA was stained with DAPI. Bar, 10 µm. (B) The Caγ-TuSC component CaSpc97-GFP was delocalized from SPBs after repression of *CaMZT1* by Dox. Δ/Tetp-*CaMZT1 CaSPC97-GFP/CaSPC97* cells were grown with and without Dox. Bar, 10 µm. (C) Time-lapse of Δ/Tetp-*CaMZT1 CaTUB1-GFP* cells with and without Dox. Time zero was set as the budding onset. See Fig. S1 F for earlier time points of cells 1 and 2. Bars, 5 µm. Enlargements of boxed areas in the time-course experiment are shown (bars, 2 µm). The arrows mark the free MTs, and the asterisks mark the neck-associated MT arrays. (D) Repression of *CaMZT1* expression led to the failure of spindle formation. Analysis of cells from C. (E) Duration of spindle assembly was estimated as interval between onset of budding and the start of spindle elongation (from C). Error bars are SEM. ***, $P < 0.001$. Ana/Telo, anaphase/telophase; M, metaphase.

(Fig. 1 C, −CaMzt1; and Video 2, cell 2) or disassembled prematurely during anaphase elongation (Video 2, cell 4). In these 15% of cells, the mean time of spindle assembly (from budding onset to short bipolar spindle) was longer than in Ca*MZT1*-expressing cells (86 vs. 65 min; Fig. 1 E). In addition, Ca*MZT1*-depleted cells rarely showed MTs that were detached from SPBs (Fig. 1 C and Fig. S1 F, −CaMzt1). Collectively, we conclude that *CaMZT1* is required for spindle assembly and integrity.

C. albicans forms filamentous hyphae upon serum treatment. Hyphal elongation and nuclear migration into the elongated hyphae rely upon cytoplasmic MTs (Finley and Berman, 2005). To test for cytoplasmic MT function, we followed hyphal formation with and without *MZT1* expression. With *CaMZT1-GFP* expression (+CaMzt1), the mean length of the induced hyphae was ∼20 µm within 2 h of serum incubation (Fig. S1, G [top] and H). The duplicated nuclei were observed within the hyphae (Fig. S1 G, top panel, white asterisks). This picture was similar in *MZT1/MZT1-GFP* wild-type cells upon serum addition regardless of Dox addition (Fig. S1 G, bottom). In contrast, upon repression of *CaMZT1-GFP* expression (−CaMzt1), the mean hyphal length was reduced to 14 µm (Fig. S1, G [top] and H). In addition, the nucleus remained in the basal cell (Fig. S1, G [red asterisks] and I), an indication of failure of nuclear migration caused by defective cytoplasmic MTs. Collectively, CaMzt1 is an SPB protein required for γ-TuSC localization at SPBs and MT function.

Caγ-TuSC has reduced self-oligomerization ability in comparison to *S. cerevisiae* γ-TuSC

To biochemically characterize the role of CaMzt1 in γ-TuSC function in vitro, we coexpressed codon-adapted γ-tubulin *CaTUB4*, *CaSPC97*, and *CaSPC98* in insect cells. The purified Caγ-TuSC contained CaSpc97, CaSpc98, and CaTub4 in a molar ratio of 1:1:2 (Fig. 2 A, right). Negative-stained protein complexes were analyzed by single-particle EM analysis and averaging of particles to compare the structures of Scγ-TuSC with those of Caγ-TuSC. The typical Y/V-shaped conformation of γ-TuSC was maintained in Caγ-TuSC (Fig. 2 B). Using 5 nm Ni-NTA-gold, we localized the 6His-tagged N termini of CaSpc97 and CaSpc98 to the base of the Y (Fig. S2 A), as is the case for the *S. cerevisiae* γ-TuSC (Choy et al., 2009; Kollman et al., 2010).

Because oligomerization of Scγ-TuSC is sensitive to the pH and salt concentration, we first tested the oligomerization level of Caγ-TuSC under different conditions by gel filtration and compared its properties with those of Scγ-TuSC (Kollman et al., 2010). In HB100 buffer, pH 7.4, Caγ-TuSC was exclusively monomeric. In contrast, Scγ-TuSC already exhibited a tendency to self-associate in this buffer system, as indicated by the breadth of the Scγ-TuSC peak and protein complexes in the void volume of the gel-filtration column (Fig. 2 C). In BRB80 buffer, pH 6.8, Scγ-TuSC formed oligomers, whereas most Caγ-TuSC precipitated; only a minor fraction ran into the column (Fig. 2 D). Caγ-TuSC oligomers were observed in the presence of 100 mM (∼30%) and 150 mM KCl (∼5%) but not in 200 mM KCl (Fig. 2 E). Negative-staining EM analysis of the Caγ-TuSC oligomers revealed uniform spherical particles with a diameter of ∼30 nm (Fig. 2 F, 100 mM KCl). In contrast to Caγ-TuSC, the majority (>90%) of Scγ-TuSC was oligomeric at 150 mM KCl and showed a variable degree of oligomerization at 200 mM KCl (Fig. 2 G). These data show that the Caγ-TuSC has a lower tendency to spontaneously assemble into oligomers than Scγ-TuSC (Fig. 2 H).

CaMzt1 promotes oligomerization of Caγ-TuSC

To characterize the properties of CaMzt1, recombinant CaMzt1 variants (GST-CaMzt1, 6His-CaMzt1, and EGFP-CaMzt1) were expressed in *Escherichia coli* and affinity purified. The gel-filtration profiles suggest that CaMzt1 forms oligomers ranging from trimers to tetramers (Fig. S3, A and B). We next tested whether Caγ-TuSC and CaMzt1 can coassemble into common complexes. When Caγ-TuSC and CaMzt1 were coexpressed in insect cells, CaMzt1 was efficiently copurified with Caγ-TuSC even when eluted with 400 mM salt from the ion-exchange column (Fig. 3 A). The resulting Caγ-TuSC–CaMzt1 complex presented essentially the same gel filtration profile as Caγ-TuSC (compare Fig. 2 C with Fig. 3 B). The CaMzt1/Caγ-TuSC intensity ratio was unaltered by gel filtration (Fig. S3 C). Thus, CaMzt1 stably bound to Caγ-TuSC. Quantification of the CaMzt1/Caγ-TuSC ratio using purified EGFP-CaMzt1 as standard suggested a subunit ratio of 1 CaMzt1 to 1 Caγ-TuSC (Fig. S3 D).

To analyze the nature of this association, we incubated Caγ-TuSC with EGFP-CaMzt1 followed by gel filtration. The mutant EGFP-CaMzt1^{D22A} was analyzed as well because a mutation in the corresponding residue of *S. pombe MZT1* leads to a conditional growth defect (Masuda et al., 2013). In HB100 buffer, CaMzt1 but not CaMzt1^{D22A} comigrated with Caγ-TuSC (Fig. 3 C). We next measured the binding affinity between CaMzt1 and Caγ-TuSC with microscale thermophoresis (MST), which is based on the change of particle mobility along a microscopic temperature gradient upon ligand binding (Jerabek-Willemsen et al., 2011). Caγ-TuSC was fluorescently labeled and maintained at a constant concentration of 150 nM. 6xHis-CaMzt1^{WT} was titrated from 0.014 to 237 µM. Binding curve fitting resulted in a dissociation constant (K_d) of ∼1.2 µM (Fig. 3 D). In contrast, the MST curve for 6xHis-CaMzt1^{D22A} was difficult to fit because of the low affinity of the interaction. We can only conclude that the K_d was >10 µM (Fig. 3, D and E). Thus, CaMzt1 binds with low micromolar affinity in a 1:1 ratio to Caγ-TuSC.

We next addressed whether CaMzt1 can induce oligomerization of Caγ-TuSC under selected buffer conditions. Caγ-TuSC and CaMzt1 were mixed with the indicated buffers and subjected to gel filtration. CaMzt1 coeluted with Caγ-TuSC in the BRB80 200 mM KCl buffer without inducing Caγ-TuSC oligomerization (Fig. 3 F, light orange). Interestingly, CaMzt1 induced Caγ-TuSC oligomerization when the salt concentration was reduced to 150 mM (Fig. 3 F, dark blue). EM analysis of the negatively stained protein complexes in the void volume revealed Caγ-TuSC oligomers with a relative constant diameter of ∼50 nm (Fig. 3 G). The Caγ-TuSC oligomerization potential at 150 mM salt was reduced by the CaMzt1^{D22A} mutation (Fig. 3 F, light blue). The ability of CaMzt1 to induce Caγ-TuSC oligomers was equally apparent with either GST-CaMzt1 or 6xHis-CaMzt1 (Fig. 3 F and Fig. S3 E). Thus, CaMzt1 is able to induce Caγ-TuSC oligomers for which diameters are too large for templating MT nucleation.

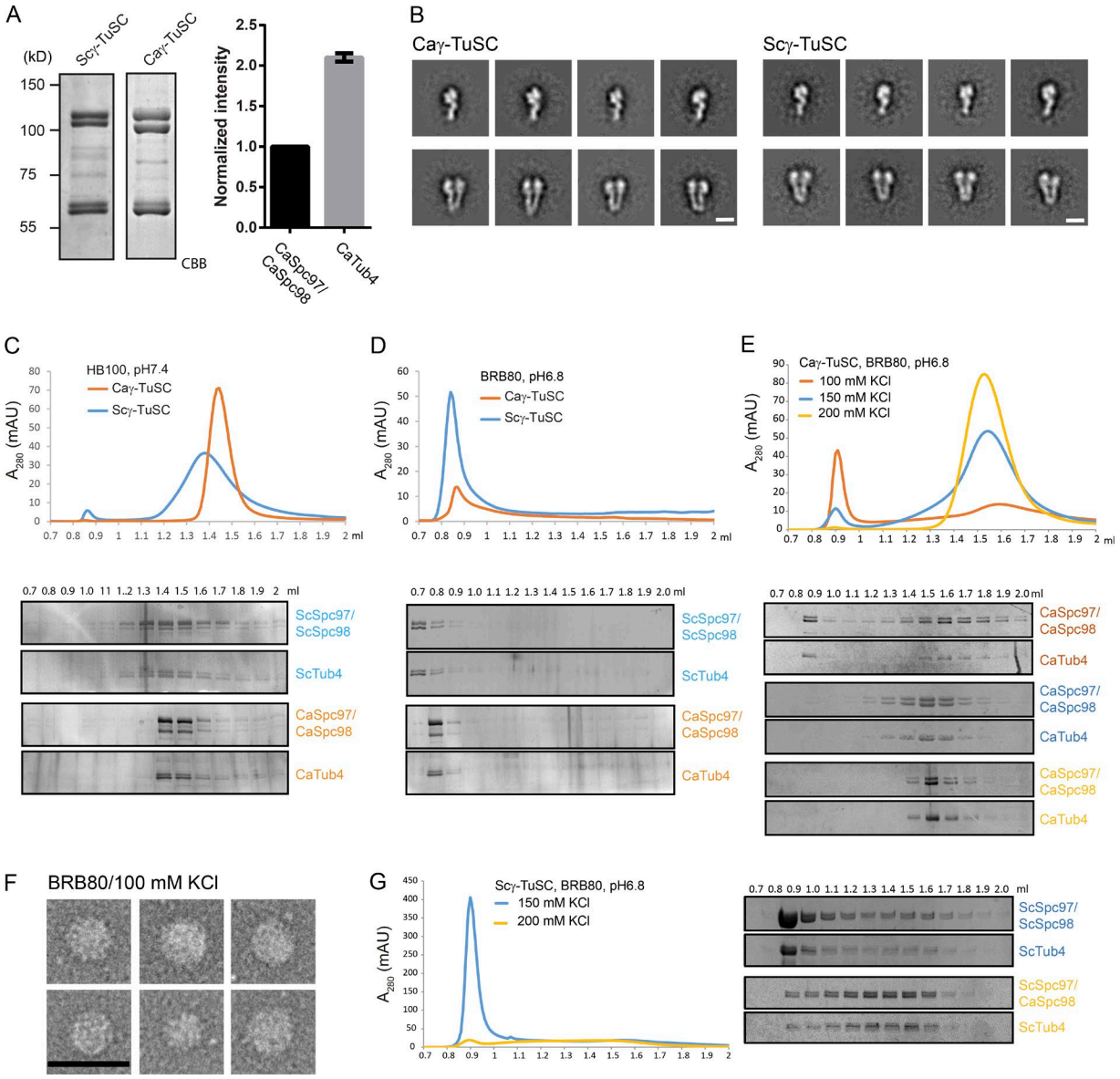

H

	Scγ-TuSC	Caγ-TuSC
HB100	Mostly monomeric form with slight multimeric tendency	Predominantly monomeric form with single peak
BRB80	Predominantly multimeric forms at void volume	Aggregration
BRB80, 100 mM KCl	Predominantly multimeric forms with single peak at void volume	Predominantly multimeric forms with single peak at void volume
BRB80, 150 mM KCl	Predominantly multimeric forms with single peak at void volume	Mostly monomeric form with slight multimeric tendency
BRB80, 200 mM KCl	Various multimeric levels with broad distribution	Predominantly monomeric form with single peak

Figure 2. **Caγ-TuSC has lower propensity to self-oligomerize than the *S. cerevisiae* γ-TuSC.** (A, left) CBB-stained gel of purified Scγ-TuSC and Caγ-TuSC. (right) Molecular ratio of CaTub4 and CaSpc97-CaSpc98 based on intensities. Error bars are SEM. $n = 5$ independent experiments. (B) Negative-stained Caγ-TuSC and Scγ-TuSC have similar structures under EM single-particle analysis. Boxed negative-stained particles were classified and averaged. See Fig. S2 B for representative micrographs. Bars, 10 nm. (C) Scγ-TuSC has higher oligomerization propensity than Caγ-TuSC. Scγ-TuSC and Caγ-TuSC were analyzed by gel filtration (Superose 6 PC3.2/30). Fractions were analyzed with SDS-PAGE and CBB. (D) As in Fig. 2 C but in the low-salt BRB80 buffer, pH 6.8. (E) Caγ-TuSC was incubated with BRB80 buffer, from 100 to 200 mM KCl, and then subjected to gel filtration. (F) Self-oligomerized Caγ-TuSC in low-salt BRB80 buffer (100 mM KCl) showed ordered spherical structures of 30 nm in diameter. Protein peak (0.9 ml) of E was analyzed by negative-staining EM. Bar, 50 nm. (G) Scγ-TuSC formed high oligomeric assemblies in BRB80 (150 mM KCl) but formed less high-mol-wt oligomers in BRB80 (200 mM KCl). SDS-PAGE with CBB. (H) Summary of buffer effect on γ-TuSC oligomerization. mAU, milli-absorbance unit.

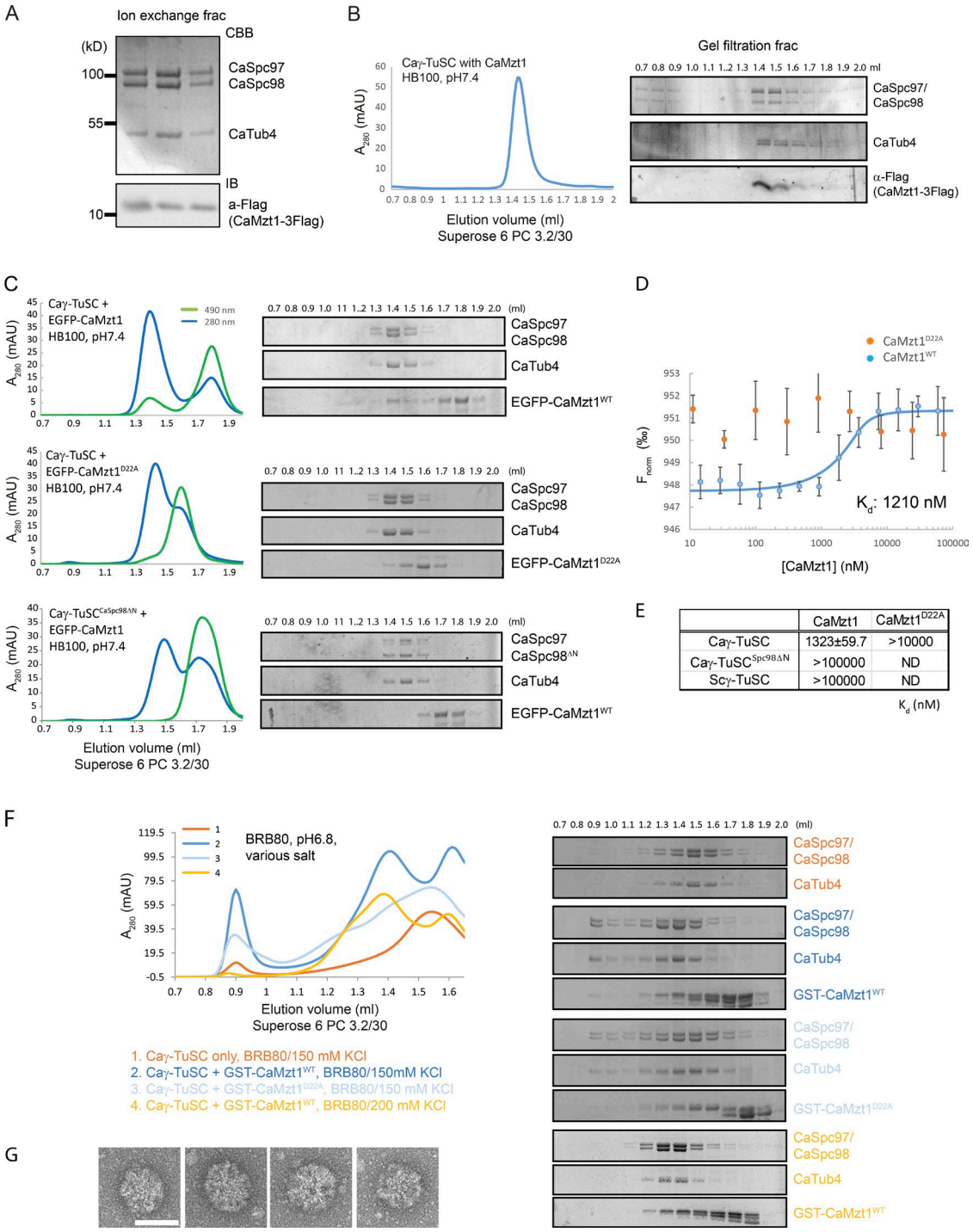

Figure 3. **CaMzt1 directly interacts with Caγ-TuSC and promotes Caγ-TuSC oligomerization.** (A) CaMzt1 forms a stable complex with Caγ-TuSC. Recombinant CaMzt1-3Flag and Caγ-TuSC were copurified. Protein complex was subjected to ion-exchange chromatography (MonoQ; gradient from 50–500 mM NaCl). Caγ-TuSC-CaMzt1 eluted at ∼400 mM NaCl; peak fractions were analyzed by SDS-PAGE. Immunoblot (IB) for 3Flag-tagged CaMzt1. (B) The purified Caγ-TuSC-CaMzt1 was stable and monomeric after ion exchange and gel filtration. SDS-PAGE with CBB; IB for 3Flag-tagged CaMzt1. (C) Caγ-TuSC–CaMzt1 interaction was reconstituted in vitro. Purified EGFP-CaMzt1 was incubated with Caγ-TuSC in HB100, pH 7.4. A_{490} detected EGFP-CaMzt1. The faint band below CaSpc97 in Caγ-TuSC$^{Spc98\Delta N}$ is a degradation product. SDS-PAGE with CBB. (D) Binding affinity between Caγ-TuSC and CaMzt1 was measured with MST. Fluorophore-labeled Caγ-TuSC and Caγ-TuSC$^{Spc98\Delta N}$ (150 nM) were incubated with CaMzt1^{WT} and CaMzt1^{D22A} ranging from ∼10 nM to ∼240 µM. Four records from two independent sample preparations were collected, and the mean values were subjected to binding curve fitting with NanoTemper software. Error bars are SD. The binding curve is a single representative out of three independent measurements. (E) Summary of MST measurements of CaMzt1 and CaMzt1^{D22A} with the indicated γ-TuSCs. K_d ± SD; n = 3 independent measurements. (F) CaMzt1 promoted Caγ-TuSC oligomerization under low-salt buffer. Recombinant CaMzt1 was incubated with Caγ-TuSC and analyzed by gel filtration, SDS-PAGE, and CBB. The control Caγ-TuSC only (150 mM KCl) is the same as shown in Fig. 2 E. (G) Oligomerization of Caγ-TuSC–CaMzt1 complexes under low-salt buffer resulted in large irregular oligomers. Peak fraction of F was subjected to negative staining and EM. Bar, 50 nm. mAU, milli-absorbance unit.

CaMzt1 and γ-TuCRs CaSpc110 and CaSpc72 interact with different regions of Caγ-TuSC

In this study, we analyzed how CaMzt1 and CaSpc72/CaSpc110 interact with Caγ-TuSC. We first localized EGFP-CaMzt1 within Caγ-TuSC by negative-stain EM analysis and averaging of the particles. Comparison of Caγ-TuSC and Caγ-TuSC–EGFP–CaMzt1 complexes by EM revealed the recruitment of EGFP-CaMzt1 to a small tail at the base of Caγ-TuSC Y/V-structure (Fig. 4 A, right). No obvious difference was observed in the structure of the main body of the Caγ-TuSC in the Caγ-TuSC–CaMzt1 complex (compare Fig. 2 B with Fig. 4 A). Nevertheless, this does not exclude the possibility of conformational changes that are beyond the resolution limit of this approach.

We next asked whether CaSpc98-N is essential and sufficient for the interaction between CaMzt1 and Caγ-TuSC. An N-terminal–truncated CaSpc98 (deletion from 1–129, CaSpc98$^{\Delta N}$) retained an intact GRIP1 domain. CaSpc98$^{\Delta N}$ did not interfere with Caγ-TuSC formation (Fig. 4 B, left), similar to ScSpc98$^{\Delta N}$ that also assembles into a stable Scγ-TuSC$^{Spc98\Delta N}$ (Lin et al., 2014). Single-particle EM analysis of Caγ-TuSC$^{Spc98\Delta N}$ showed the typical Y/V conformation (Fig. 4 B, right). Interestingly, Caγ-TuSC$^{Spc98\Delta N}$ failed to interact with EGFP-CaMzt1 by gel filtration (Fig. 3 C), and the K_d value was estimated to be >100 µM in the MST analysis (Fig. 3 E).

Scγ-TuSC could not interact with EGFP-CaMzt1 (Figs. 3 E and 4 C). To confirm that the CaSpc98-N determines the binding of Caγ-TuSC to CaMzt1, we swapped the amino termini of the Spc98's of *S. cerevisiae* and *C. albicans* to construct chimeric forms of Spc98 (CaN-ScSpc98 and ScN-CaSpc98). Ni-NTA purification from insect cells expressing Caγ-TuSC$^{ScSpc98\text{-}N}$ and CaMzt1 did not reveal interaction, whereas Scγ-TuSC$^{CaSpc98\text{-}N}$ copurified with CaMzt1 (Fig. 4 D). The Scγ-TuSC$^{CaSpc98\text{-}N}$–CaMzt1 interaction was intact during ion-exchange purification of the complex (Fig. S3 F). The Scγ-TuSC$^{CaSpc98\text{-}N}$–CaMzt1 interaction was confirmed by incubating purified Scγ-TuSC$^{CaSpc98\text{-}N}$ with EGFP-CaMzt1 followed by gel-filtration analysis (Fig. 4 C, right, peak at 1.45-ml elution volume in the GFP channel). In contrast, Caγ-TuSC$^{ScSpc98\text{-}N}$ failed to interact with EGFP-CaMzt1, yet now strongly oligomerized in HB100 buffer (Fig. 4 C, middle), a property that was not observed for Caγ-TuSC in this buffer (Fig. 2 C). Thus, the N-terminal 129 aa of CaSpc98 are required and sufficient to confer γ-TuSC binding to CaMzt1.

To determine whether CaMzt1 and the γ-TuCRs bind to the same N-terminal region of CaSpc98 within Caγ-TuSC, we purified the N-terminal fragments of *C. albicans* Spc110 or Spc72 fused with the GST-tag (GST–CaSpc110-N: 1–222; GST–CaSpc72-N: 1–420) from *E. coli*. Although the CaSpc110-N encompasses the putative Spc110/Pcp1 motif (SPM) and CM1 elements, the CaSpc72-N only has the short CM1 (Fig. S4, A and B). The GST-tag mimics the dimerization state of the γ-TuCRs, which is conferred in the full-length proteins by the central coiled-coli region (Lin et al., 2014). In addition, it has been shown that higher-order oligomerization of ScSpc110-N is essential to promote Scγ-TuSC oligomerization (Muller et al., 2005; Lyon et al., 2016). Importantly, the binding of Caγ-TuSC-$^{Spc98\Delta N}$ to CaSpc110-N and CaSpc72-N was not perturbed, as demonstrated in MST measurements (Fig. S4 C). In fact, CaSpc110-N and CaSpc72-N bound with a slightly higher affinity to Caγ-TuSC$^{Spc98\Delta N}$ than to Caγ-TuSC. Because CaMzt1 does not interact with Caγ-TuSC$^{Spc98\Delta N}$, this demonstrates that CaMzt1 and γ-TuCRs bind to different domains of Caγ-TuSC. In addition, MST measurements and gel-filtration analysis showed that ScSpc110-N bound to Caγ-TuSC with high affinity without inducing oligomerization (Fig. 4, E and F, middle; and Fig. S4 C). This suggests that ScSpc110-N has retained the ability to interact with Caγ-TuSC. Nevertheless, probably because of the reduced oligomerization properties of Caγ-TuSC, no oligomer was formed. In contrast, ScSpc110-N induced Scγ-TuSC oligomerization in the same buffer system (Fig. 4 F, right). Interestingly, the binding affinity of ScSpc110-N to Scγ-TuSC was ∼20-fold higher than CaSpc110-N binding to Caγ-TuSC (Fig. S4 C), suggesting an adaptation of the *S. cerevisiae* MT nucleation system to the lack of Mzt1 homologue.

CaMzt1 interacts with CaSpc110 and CaSpc72 depending on their CM1 element

Both γ-TuCRs and Mzt1/MOZART1 are required to target γ-tubulin complexes to MTOCs in different model organisms, raising the possibility of direct interaction between them. Indeed, in gel filtration, the addition of CaSpc110-N shifted the elution profile of EGFP-CaMzt1 toward a higher molecular weight structure (Fig. 5 A, right curve), indicating that CaSpc110-N directly interacts with CaMzt1. The binding affinity between wild-type EGFP-CaMzt1 and CaSpc110-N (1–222 aa) was quantified with MST analysis, resulting in a K_d of ∼200 nM (Fig. 5, C and E). In contrast, the mutant EGFP-CaMzt1^{D22A} showed six times reduced binding affinity to CaSpc110-N (Fig. 5 C). Interestingly, CaMzt1-EGFP showed three times lower binding affinity to CaSpc110-N than EGFP-CaMzt1, indicating some interference of CaMzt1 by C-terminal tagging (Fig. 5 C). We therefore used EGFP-CaMzt1 in all subsequent measurements.

As Spc110-N of *S. cerevisiae*, the CaSpc110-N expressed in insect cells was phosphorylated within the region between the SPM and CM1 motifs (Fig. S4, A and D; Lin et al., 2014). However, the corresponding phospho-mimetic CaSpc110-N mutants did not alter the binding to CaMzt1 (Fig. S4 E), suggesting that such phosphorylations in CaSpc110 do not affect CaMzt1 binding or that the mutations did not faithfully mimic the effect of phosphorylation.

ScSpc110-N did not display any measurable affinity for CaMzt1 in the MST quantification (Fig. 5, D and E), an indication for the loss of the Mzt1 binding site. Because CaSpc110-CM1 and ScSpc110-CM1 only share 44% similarity, we next asked whether the CM1 motif of CaSpc110 is important for CaMzt1 binding. We noticed that CM1 of γ-TuCRs (except for Spc72; Fig. S4 B) is potentially composed of two duplicated motifs, CM1a and CM1b, which share a similar motif pattern (2ζ-Φ-X-K-E-N-Φ-ζ-L-K-X-ζ-3X-L-3ζ-L; Φ: hydrophobic; ζ: hydrophilic; Fig. 5 B, underlined; and Fig. S4 F). To analyze binding of CaMzt1 and Caγ-TuSC to CaSpc110-CM1, we constructed three mutant versions of CaSpc110-N: CaSpc110-N^{9A1}, CaSpc110-N^{9A2}, and CaSpc110-N^{4A}, which harbor mutations in CM1a, CM1b, and both, respectively (Fig. 5 B, blue, orange, and red asterisks for 9A1, 9A2, and 4A, respectively; 1–222 aa for all constructs). CaSpc110-N^{9A1} and CaSpc110-N^{9A2} did not affect binding to CaMzt1 (Fig. 5 D). In contrast, CaSpc110-N^{4A} abolished the interaction with CaMzt1 (Fig. 5, D and E). Interestingly, CaSpc110-N^{9A2} reduced the affinity to Caγ-TuSC by a factor of 6, whereas CaSpc110-N^{9A1} and CaSpc110-N^{4A} had similar or even slightly enhanced binding to Caγ-TuSC compared with CaSpc110-N^{WT} (Fig. 4 E). Thus,

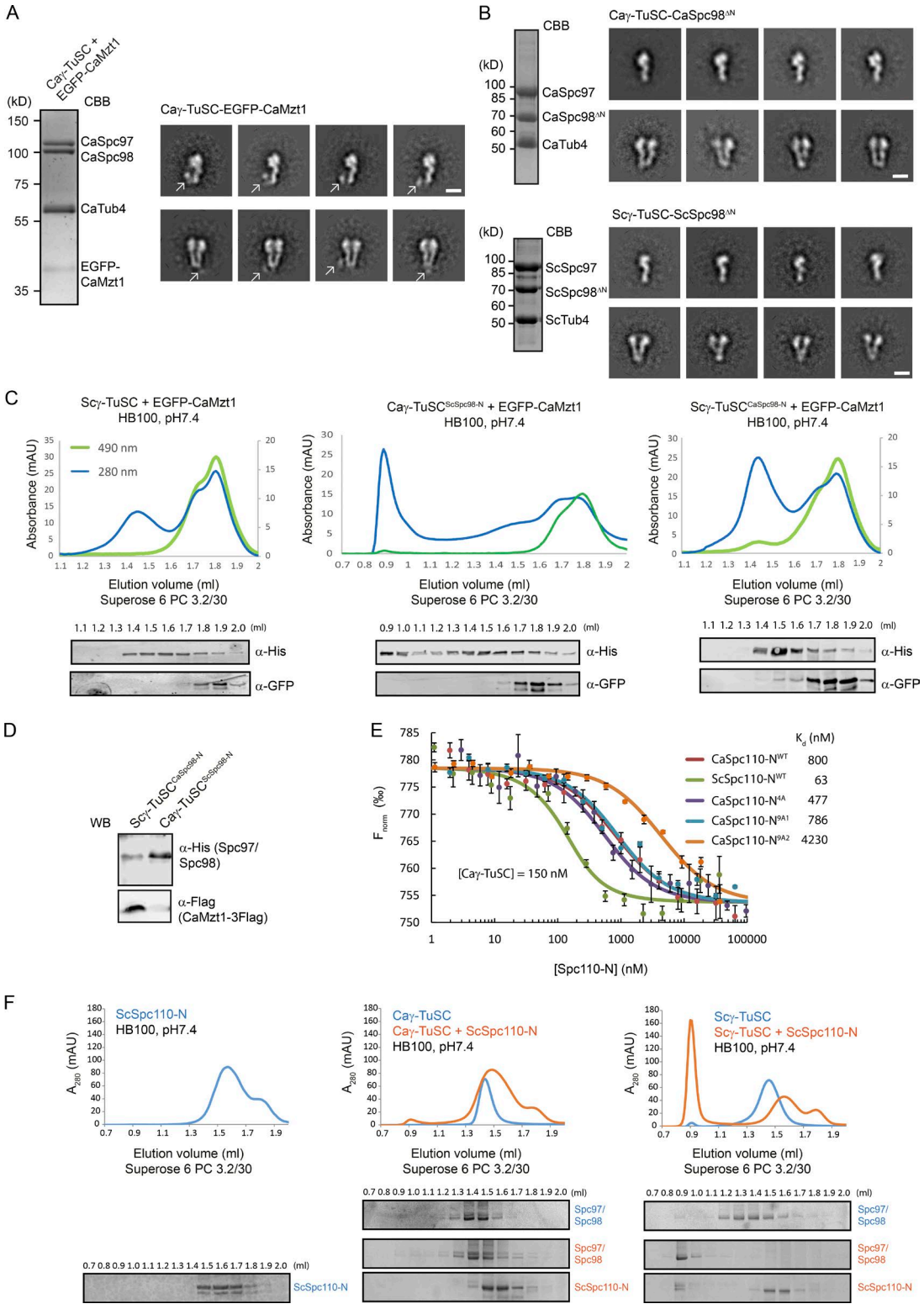

Figure 4. **CaMzt1 directly interacts with the N-terminal domain of CaSpc98.** (A) EGFP-CaMzt1 is located near the tail at the base of Cαγ-TuSC. Left: CBB-stained gel. Right: boxed negative-stained Cαγ-TuSC-EGFP-CaMzt1 particles were classified and averaged. The arrows point to the additional density of EGFP-CaMzt1. Bar, 10 nm. (B) The deletion of N-terminal domain of Spc98 did not affect γ-TuSC assembly. Purified Cαγ-TuSC$^{Spc98\Delta N}$ and Scγ-TuSC$^{Spc98\Delta N}$ (left) were subjected to negative staining and EM analysis (right). Bars, 10 nm. (C) The CaSpc98-N determines binding of Cαγ-TuSC to CaMzt1. Gel filtration of EGFP-CaMzt1 incubated with purified Scγ-TuSC, Cαγ-TuSC$^{ScSpc98\text{-}N}$, and Scγ-TuSC$^{CaSpc98\text{-}N}$. Immunoblot of elution fractions with anti-His (for Spc97 and Spc98) and anti-GFP (for CaMzt1). (D) CaMzt1-3Flag was copurified with Scγ-TuSC$^{CaSpc98\text{-}N}$ but not to Cαγ-TuSC$^{ScSpc98\text{-}N}$. γ-TuSCs were purified with Ni-NTA and analyzed with SDS-PAGE. Western blots (WB) are shown. (E) Binding affinity between Cαγ-TuSC and Spc110-N by MST, as in Fig. 3 D. Error bars are SD. (F) The ScSpc110-N binds both Scγ-TuSC and Cαγ-TuSC but promotes oligomerization of only Scγ-TuSC. As in C. SDS-PAGE and CBB. mAU, milli-absorbance unit.

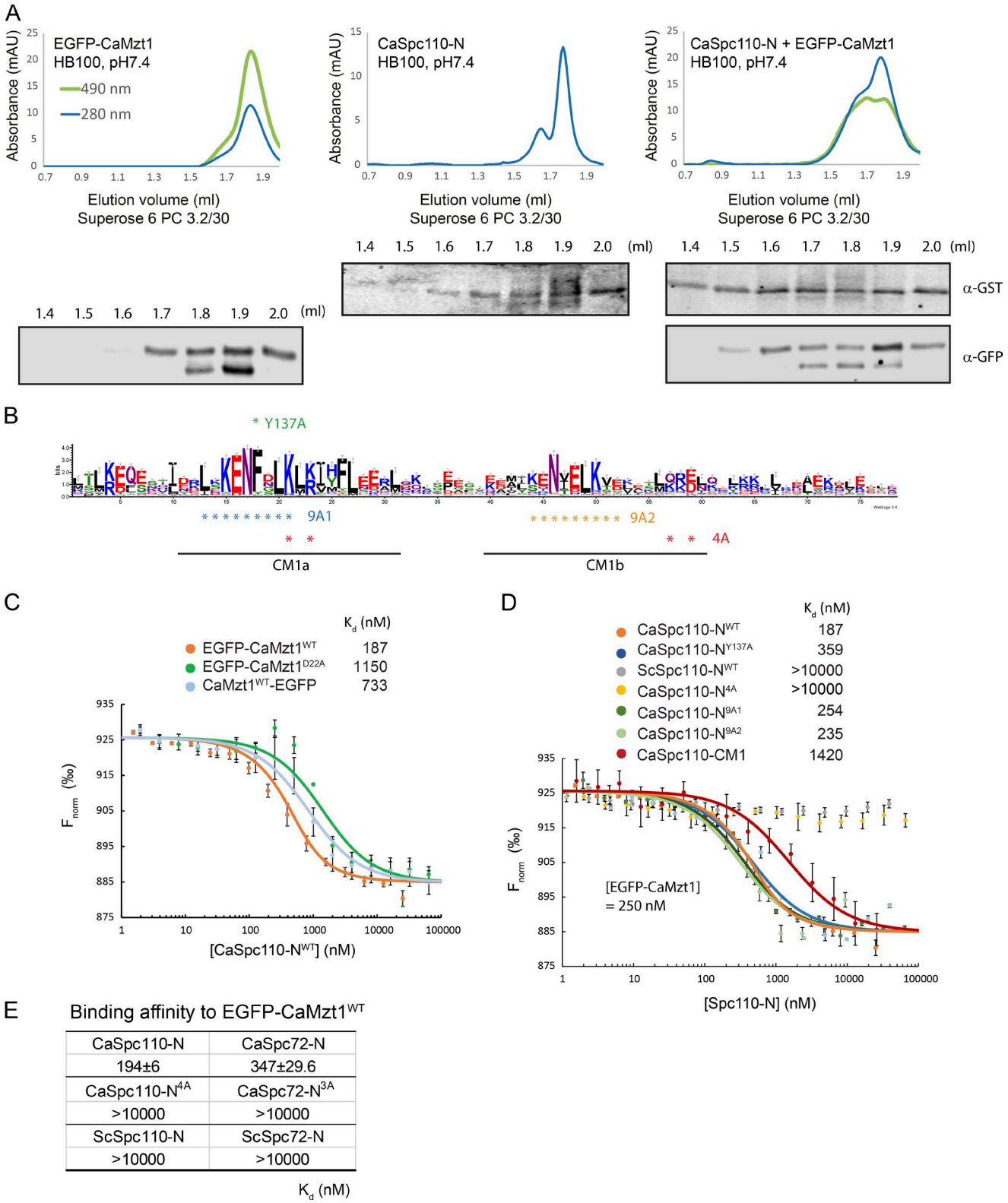

E

Binding affinity to EGFP-CaMzt1^{WT}

CaSpc110-N	CaSpc72-N
194±6	347±29.6
CaSpc110-N^{4A}	CaSpc72-N^{3A}
>10000	>10000
ScSpc110-N	ScSpc72-N
>10000	>10000

K_d (nM)

Figure 5. **CaMzt1 interacts with CaSpc110-N and CaSpc72-N depending on the CM1 element.** (A) CaMzt1 directly interacts with CaSpc110-N. Mixed EGFP-CaMzt1 and GST–CaSpc110-N were subjected to gel filtration. Analysis as in Figs. 3 C and 4 C. The bottom band in the anti-GFP blot is an EGFP-CaMzt1 degradation product. (B) Weblogo of CM1 element of γ-TuCRs. CM1a and CM1b are underlined. Green asterisk marks Y137A. Red asterisks indicate mutated residues in CaSpc110-N^{4A}. Mutations in CaSpc110-N^{9A1} and CaSpc110-N^{9A2} are marked blue and orange, respectively. (C) MST measurement of the binding of EGFP-CaMzt1, EGFP-CaMzt1^{D22A}, or CaMzt1-EGFP to CaSpc110-N^{WT} (1–222 aa). Error bars are SD. Single representative binding curve out of three independent experiments is shown. (D) MST measurement of the binding of EGFP-CaMzt1 to CaSpc110-N variants. Error bars are SD. Single representative binding curve out of three independent experiments is shown. (E) Summary of MST measurements on the binding of EGFP-CaMzt1 to CaSpc72-N and CaSpc110-N. K_d ± SD; n = 3 independent measurements. mAU, milli-absorbance unit.

binding of CaSpc110-N to CaMzt1 and Caγ-TuSC requires different amino acid residues within the CM1 (Fig. S4 G). Next, we tested whether the CM1 was sufficient to mediate binding to CaMzt1. Purified short CaSpc110^{CM1} fragment (117–176 aa) did not give equally high affinity to CaMzt1 as CaSpc110-N^{WT} (1–222 aa; Fig. 4 D; K_d = 1,420 vs. 187 nM), suggesting that regions in addition to CM1 are required for high-affinity binding of CaSpc110-N to CaMzt1. Thus, the CaSpc110 CM1 is essential but not sufficient for CaMzt1 high-affinity binding.

In comparison with CaSpc110-N, the *C. albicans* CaSpc72-N shifted the elution profile of EGFP-CaMzt1 to a lesser extent in gel filtration (Fig. S5 A). MST affinity measurements demonstrated that the binding affinity of CaSpc72-N to EGFP-CaMzt1 was half that of CaSpc110-N (Fig. S5 B). Furthermore, mutation of three conserved residues within the short CM1 (CaSpc72-N^{3A}: K251A-Q253A-K255A; Fig. S4 F) reduced CaSpc72^{3A} binding to EGFP-CaMzt1 (Fig. S5 B, top) without affecting the high-affinity binding to Caγ-TuSC (Fig. S5 B, bottom). However, a more extensive CaSpc72-N^{9A} in the CM1 (Fig. S4 F) reduced interaction with CaMzt1 and Caγ-TuSC (Fig. S5 B).

Collectively, our results demonstrated that CaSpc110-N and CaSpc72-N directly interact with CaMzt1 depending on the integrity of the CM1 element, which is also required for Caγ-TuSC binding.

CaMzt1 and CaSpc110 cooperate in the assembly of active γ-TuSC rings

To test whether Caγ-TuSC, CaMzt1, and the γ-TuCRs assemble into stable complexes, we coexpressed GST–CaSpc110-N and Caγ-TuSC with and without CaMzt1 in insect cells and purified any resulting complexes using the GST-tag (Fig. 6 A). Gel-filtration analysis revealed cofractionation of CaMzt1, CaSpc110-N, and Caγ-TuSC in one complex (Fig. 6 B). Moreover, MST analysis indicated that CaSpc110-N bound with three times higher affinity to the preassembled Caγ-TuSC–CaMzt1 complex than to Caγ-TuSC (Fig. 6 C). We conclude that CaMzt1, CaSpc110-N, and Caγ-TuSC assemble into stable complexes and that CaMzt1 enhances the binding of CaSpc110-N to Caγ-TuSC.

CaMzt1 did not oligomerize Caγ-TuSC in HB100 buffer (Fig. 3, B and C). In contrast, under this buffer condition, CaMzt1 did promote the oligomerization of Caγ-TuSC–CaSpc110-N approximately threefold when compared with the control that lacked CaMzt1 (Fig. 6 B). This suggests that CaMzt1 and CaSpc110 cooperate in promoting the oligomerization of Caγ-TuSC. Next, we analyzed the oligomers in the peak at void volume of the gel filtration with negative staining and EM analysis (Fig. 6 D). In contrast to the well-organized spiral-like structures of the Scγ-TuSC–Spc110-N oligomers (Kollman et al., 2010), Caγ-TuSC–CaSpc110-N oligomers were heterogeneous, presenting irregular ringlike structures with a mean diameter of 46 nm (Fig. 6, D and E). Strikingly, in the presence of CaMzt1, the oligomerized Caγ-TuSC–CaSpc110-N–CaMzt1 complexes showed more homogenous and compact ringlike structures with a mean diameter of ∼30 nm (Fig. 6 D), compatible with the diameter of 13-protofilament MTs (∼25 nm). In addition, the individual spokelike Caγ-TuSC subunits were well organized. Collectively, we conclude that CaMzt1 and CaSpc110-N are both required to assemble Caγ-TuSC into ∼30-nm ringlike structures.

We next asked whether CaSpc72-N also cooperates with CaMzt1 in the interaction with Caγ-TuSC and the induction of Caγ-TuSC oligomers. In contrast to CaSpc110-N, CaSpc72-N showed similar binding affinities to Caγ-TuSC and Caγ-TuSC–CaMzt1 complexes (Fig. 6 C). Despite this lack of enhancement in binding affinity, only the combined addition of CaMzt1 and CaSpc72-N promoted Caγ-TuSC oligomerization in HB100, pH 7.4, buffer (Fig. S5 C). Thus, CaSpc72-N also cooperates with CaMzt1 in Caγ-TuSC oligomerization.

The EM data suggest that it is only through cooperation of γ-TuCRs with CaMzt1 that Caγ-TuSC gains the ability to assemble into MT nucleation-competent rings. We tested this model by analyzing the MT nucleation activity of assembled Caγ-TuSC oligomers in vitro. The single addition of CaMzt1, CaSpc72-N, or CaSpc110-N alone did not significantly increase the MT nucleation compared with Caγ-TuSC alone. Strikingly, when CaMzt1 and the receptor N-terminal fragments were combined, nucleation activity increased 5–13-fold in comparison with Caγ-TuSC alone (Fig. 6 F). The synergistic impact arising from the interaction of the receptor and CaMzt1 with Caγ-TuSC is needed to obtain active MT nucleation platforms.

To test the cooperation of CaSpc110-N, CaSpc98-N, and CaMzt1 in an in vivo environment, we asked which of these elements are required to target EGFP-CaMzt1 to the *S. cerevisiae* SPB. We constructed chimeric mutants of *SPC98* and *SPC110* (*ScSPC98$^{CaSpc98\text{-}N}$* and *ScSPC110$^{CaSpc110\text{-}N}$*), of which the N-terminal domain was changed to CaSpc98-N and CaSpc110-N, respectively. Although the *ScSPC110$^{CaSpc110\text{-}N}$* failed to complement the essential function of Sc*SPC110*, *ScSPC98$^{CaSpc98\text{-}N}$* complemented *ScSPC98Δ* (Fig. S5 E). Thus, experiments were performed in *ScSPC110$^{CaSpc110\text{-}N}$ ScSPC110* cells expressing either *ScSPC98* or *ScSPC98$^{CaSpc98\text{-}N}$*. EGFP-CaMzt1 failed to be recruited to the SPB of *S. cerevisiae* cells that only expressed Sc*SPC98 ScSPC110, ScSPC98$^{CaSpc98\text{-}N}$ ScSPC110*, or *ScSPC98 ScSPC110$^{CaSpc110\text{-}N}$* (Fig. 6 G). Interestingly, EGFP-CaMzt1 showed SPB localization when *ScSPC98$^{CaSpc98\text{-}N}$* and *ScSPC110$^{CaSpc110\text{-}N}$* were coexpressed (Fig. 6 G). This experiment shows that only CaSpc110-N in combination with CaSpc98-N targets CaMzt1 to the SPB in an in vivo situation.

Collectively, our results demonstrate that the γ-tubulin complex–targeting factors CaMzt1 and CaSpc110-N cooperate to promote Caγ-TuSC oligomerization and direct the assembly of an active MT nucleation template.

Human MOZART1 directly interacts with CEP215-N and is important for γ-TuRC stability

To ask whether our finding in *C. albicans* can be applied in higher eukaryotes, we first tested the interaction between human MOZART proteins (MOZART1 and MOZART2b) and the N-terminal extensions of GCP proteins in the yeast two-hybrid system. MOZART1 associated with the N-terminal half of GCP3, GCP5, and GCP6 but with neither GCP4, which lacks N-terminal extension, nor GCP2 (Fig. 7 A). MOZART2b only interacted with GCP2-N in this system. This suggests the GCP-N interaction with MOZART1/Mzt1 is most likely conserved in humans.

Next, we tested if the Mzt1–γ-TuCR interaction is conserved in humans. MOZART1 was coimmunoprecipitated with CEP215, the human γ-TuCR with CM1 motif (Fig. 7 B), suggesting the presence of such an interaction. To verify and quantify the MOZART1–CEP215 interaction, MST experiments were performed with purified MOZART1 and the N-terminal,

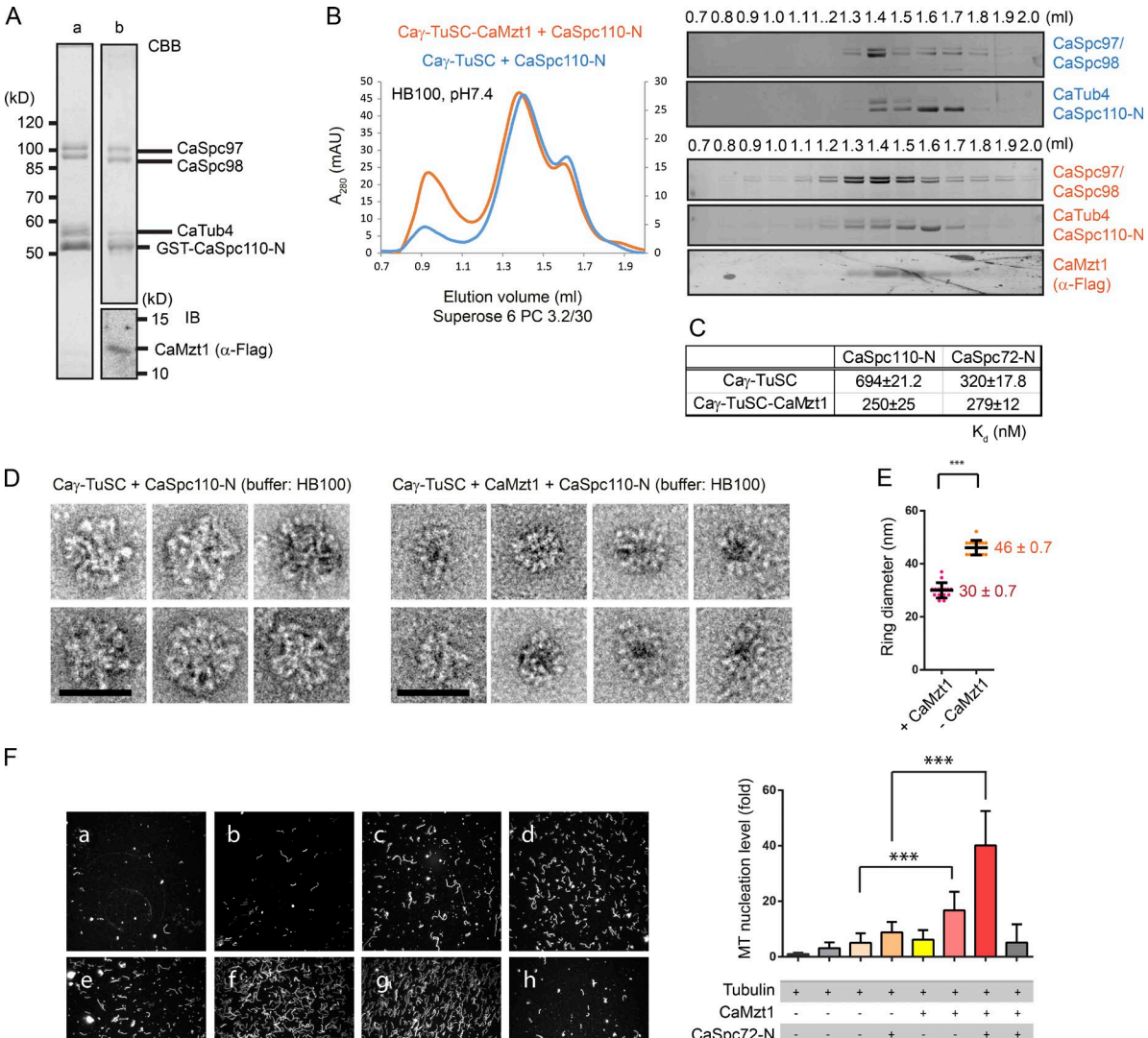

Figure 6. **Mzt1 is dispensable for the binding of γ-TuSC to receptors but required for the assembly of active γ-TuSC rings.** (A) Cαγ-TuSC was copurified with CaSpc110-N with (b) and without (a) CaMzt1. The purified complexes were eluted from GST-resin. SDS-PAGE (CBB) and anti-Flag immunoblot (IB; CaMzt1-3Flag) are shown. (B) Coexpression of CaMzt1 and CaSpc110-N promotes oligomerization of Cαγ-TuSC. The presence of CaMzt1 further increased oligomerization. Complexes from A were subjected to gel-filtration analysis. SDS-PAGE with CBB. (C) CaSpc110-N has higher affinity to Cαγ-TuSC–CaMzt1 than Cαγ-TuSC alone. MST was performed as in Fig. 3 C. K_d ± SD; n = 3 independent measurements. (D) CaMzt1 keeps the oligomerization of Cαγ-TuSC–CaSpc110-N compact and organized. Cαγ-TuSC–CaSpc110-N and CaMzt1–Cαγ-TuSC–CaSpc110-N complexes from void (0.9 ml) in B were subjected to negative staining and EM. Bars, 50 nm. (E) The averaged diameter of Cαγ-TuSC–CaSpc110-N oligomers was larger than oligomers with CaMzt1. Error bars are SD. n = 15 (number of particles measured in each sample). ***, P < 0.001 with t test. (F) CaMzt1 is required for optimal MT nucleation activity. Left: maximum projection of 20 images for each sample. Bar, 50 µm. Right: statistical analysis of MT nucleation. n = 6–9 independent samples from 3 independent experiments. Error bars are SD. ***, P < 0.001. Fig. S5 D shows DMSO and taxol control. (G) The N-terminal domains of CaSpc98 and CaSpc110 are both required to recruit CaMzt1 to *S. cerevisiae* SPBs. *EGFP-CaMZT1* expression was induced with galactose. Spc42-mCherry is an SPB marker. Bar, 5 µm. Ana, anaphase; M, metaphase.

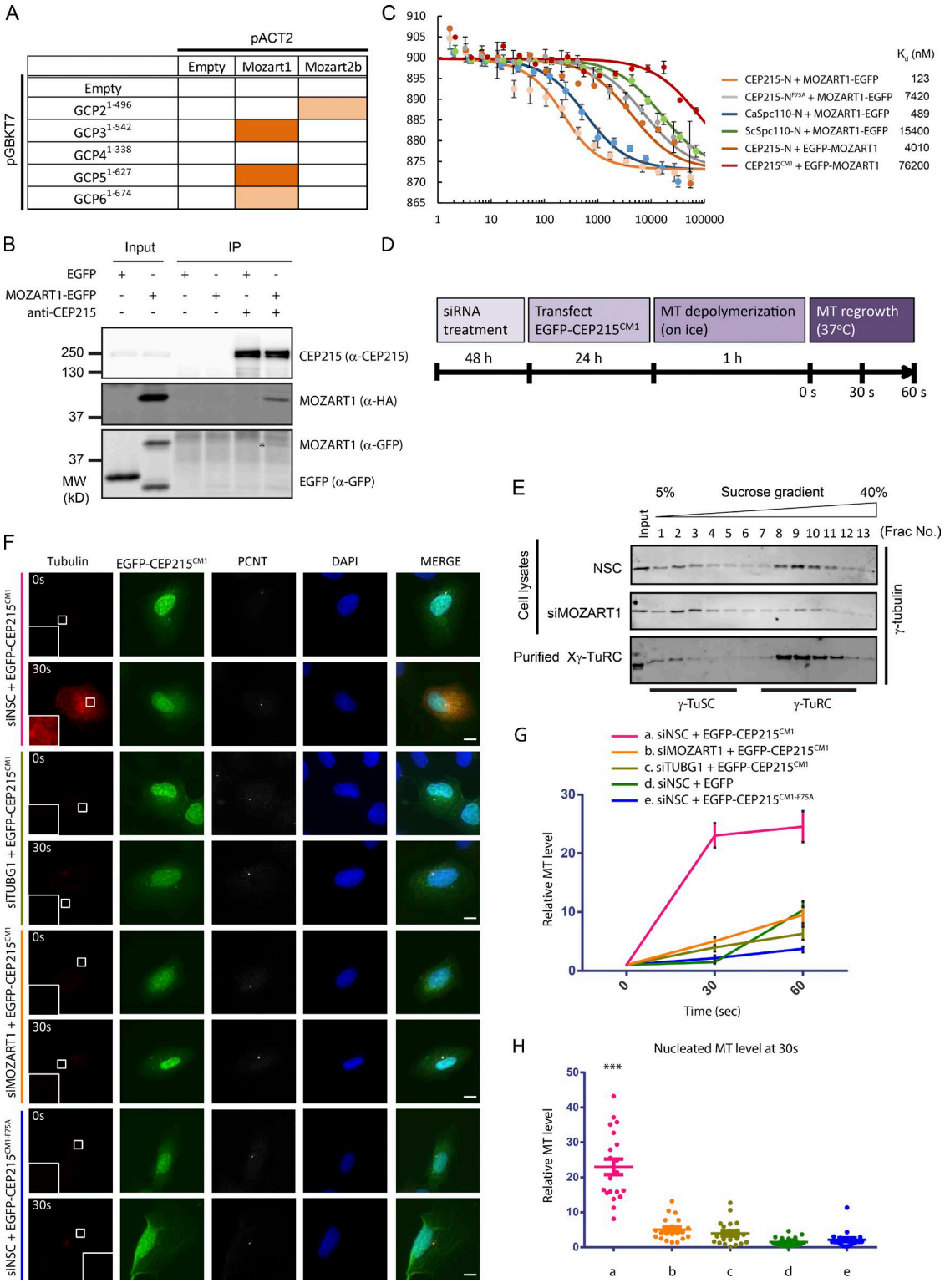

Figure 7. **MOZART1 binds to CEP215-N in dependence of CM1 and stabilizes the γ-TuRC.** (A) Summary of yeast two-hybrid analysis. Dark orange is strong; light orange is mild; and white is no interaction. (B) MOZART1 interacts with CEP215. MOZART1-EGFP was coimmunoprecipitated (IP) with CEP215. Immunoblotted with indicated antibodies. Asterisk marks the band of MOZART1-EGFP blotted with anti-GFP. (C) The CM1 of CEP215 is required for interaction with human MOZART1. MST measurements as in Fig. 3 D. Error bars are SD. The fitting curves shown are from a single representative experiment out of three independent experiments. (D) Experimental scheme of knockdown of MOZART1 and in vivo MT nucleation assay. (E) γ-TuRC was destabilized after knockdown of MOZART1. After siRNA treatment (siMOZART1 and NSC), total U2OS cell lysates were separated with sucrose gradients (5–40%). γ-TuRC purified from *Xenopus* egg extract (Xγ-TuRC) was used as reference. Each fraction was resolved by SDS-PAGE followed by immunoblotting. (F) Cells showing MT disassembly upon cold treatment (0 s) and ectopic MT nucleation after 30 s of warming up. Bars, 10 µm. Insets within images of tubulin channel show the enlargement of a selected area (6.425 × 6.425 µm^2). (G) Ectopic MT nucleation from F was quantified as described in Materials and methods. n = 20 cells analyzed. Error bars are SEM. (H) MT intensities after 30 s. Error bars are SEM. ***, $P < 0.001$.

CM1-containing domain of CEP215 (GST-CEP215-N, 1–220 aa). Interestingly, different from the CaSpc110-N–CaMzt1 interaction, CEP215-N interacted with the C-terminal EGFP-tagged MOZART1 (MOZART1-EGFP) significantly better than N-terminal EGFP-tagged MOZART1 (EGFP-MOZART1; K_d = 123 vs. 4,010 nM; Fig. 7 C), indicating a specific requirement of the N-MOZART1 that was blocked by EGFP. In addition, although the single mutation on the conserved residue (Y137A) within the CM1 of CaSpc110 still kept high-affinity binding of CaSpc110-N to CaMzt1 (K_d = 359; Fig. 5 D), the corresponding mutation in CEP215-N (F75A), which impairs the ability of $CEP215^{CM1}$ to stimulate MT nucleation (Choi et al., 2010), strongly reduced binding to MOZART1 (K_d = 7,420; Fig. 7 C). However the purified $CEP215^{CM1}$ (51–135 aa) lost the binding affinity to MOZART1, indicating that regions in addition to $CEP215^{CM1}$ are required for the binding to MOZART1. Further supporting the conservation of Mzt1–γ-TuCR interaction from yeast to human, CaSpc110-N showed moderate binding affinity to MOZART1-EGFP (K_d = 489 nM), whereas ScSpc110-N lost such affinity (K_d = 15,400 nM). Thus, MOZART1 directly interacts with CEP215-N, and the CM1 is required for such an interaction.

Following the scheme outlined in Fig. 7 D, we studied how siRNA depletion of MOZART1 (Hutchins et al., 2010) in human U2OS cells affects γ-TuRC stability and nucleation activity. Using an established siRNA (Hutchins et al., 2010), depletion of MOZART1 by 70% (Fig. S5 F) destabilized the γ-TuRC and gave rise to an increasing amount of γ-TuSC as indicated by the shift of γ-tubulin in a sucrose gradient upon MOZART1 depletion (Fig. 7 E). MOZART1 depletion was accompanied by inactivation of the MT nucleation activity of γ-TuRC. It has been shown that expression of $CEP215^{CM1}$ induces MT asters through activation of cytoplasmic γ-TuRCs (Choi et al., 2010). Although in the control cells (nonspecific control siRNA [siNSC] + and EGFP-$CEP215^{CM1}$) cytoplasmic asters emerged after 30-s warming up and reached plateau within 60 s (Fig. 7, F–H, sample a), depletion of MOZART1 completely abolished the $CEP215^{CM1}$-induced MT aster formation (Fig. 7, F–H, sample b). The reduction on the MT aster level upon MOZART1 depletion was the same as depletion of γ-tubulin (80% depletion; Fig. S5 F) or the expression of inactive $CEP215^{CM1\text{-}F75A}$ (Fig. 7, F–H, samples c and e). Thus, MOZART1 depletion leads to γ-TuRC disassembly, which is accompanied by loss of $CEP215^{CM1}$-induced MT nucleation activity.

Discussion

Three-way interactions among γ-TuCRs, γ-TuSC, and MOZART1/Mzt1

MOZART1/Mzt1 orthologues share conserved functions in different model organisms analyzed to date. The delocalization of γ-tubulin from MTOCs is the typical phenotype upon inactivation of MOZART1/Mzt1 orthologues (Hutchins et al., 2010; Janski et al., 2012; Nakamura et al., 2012; Dhani et al., 2013; Masuda et al., 2013). Consistently, in *C. albicans*, depletion of CaMzt1 significantly reduced γ-tubulin signal at SPBs. In addition, MOZART1/Mzt1 orthologues analyzed so far interact with GCP3 (Janski et al., 2012; Nakamura et al., 2012; Dhani et al., 2013). In this study, we show that CaMzt1 binds directly to the N-terminal extension of CaSpc98, which is at the base of the γ-TuSC Y/V as shown by EM analysis. Our yeast two-hybrid data suggest that human MOZART proteins may differentially bind GCP-Ns. Human MOZART1 interacts in this system with GCP5-N and GCP6-N in addition to GCP3-N, whereas MOZART2 interacts exclusively with GCP2-N. This is consistent with the observation that LAP-tagged MOZART2b pulled down GCP2 more efficiently than GCP3 (Hutchins et al., 2010). The absence of an N-terminal extension of the GRIP1 domain may explain why GCP4 failed to interact with MOZART proteins.

CaMzt1 and Caγ-TuCRs bind to different regions of Caγ-TuSC. Although the N-terminal domain of CaSpc98 determines the ability of Caγ-TuSC to interact with CaMzt1, it is dispensable for the interaction with CaSpc72 and CaSpc110, suggesting that Caγ-TuCRs bind to a more central portion of CaSpc97 and CaSpc98. CryoEM data (Kollman et al., 2010) indicate that the binding site of ScSpc110-CM1 is most likely located in the N-terminal regions of Spc97/GCP2 and/or Spc98/GCP3 that harbor the conserved GRIP1 domains.

The highly conserved N-terminal CM1 element of γ-TuCRs was first noticed in the Mto1 of *S. pombe* (Sawin et al., 2004). In *S. cerevisiae*, ScSpc110-CM1 mediates direct binding to γ-TuSC, and mutations within the CM1 compromised the recruitment of γ-TuSC to SPBs and the γ-TuSC oligomerization (Lin et al., 2014). In human cells, CEP215-CM1 stimulates the MT nucleation activity of γ-TuRC (Choi et al., 2010). In this study, we report that in both *C. albicans* and humans, the integrity of the CM1 element of γ-TuCRs is required for the direct binding to MOZART1/Mzt1. Although we have shown that CM1 of CaSpc110 and CaSpc72 are also required for the binding to Caγ-TuSC (Fig. 8), it is still unclear whether this is also the case for the human γ-TuRC. The finding that the CM1 of CEP215 is able to stimulate MT nucleation activity of γ-TuRC although this minimal CM1 does not interact with MOZART1 by MST, suggests a second binding site of the CM1 within the γ-TuRC. The interacting proteins may well be GCP components as is the case for the yeast γ-TuSC-γ-TuCR interaction.

The dual interaction of CaMzt1 with CaSpc98-N and CaSpc110 indicates that it clamps the Caγ-TuSC and CaSpc110 together (Fig. 8). By providing binding sites for both γ-TuCRs and CaSpc98-N, CaMzt1 also increases the affinity of the interaction between receptors and γ-TuSC. Interestingly, CaSpc98-N and CaSpc110-N are both required to recruit CaMzt1 at SPBs in *S. cerevisiae,* suggesting that CaSpc98-N, CaSpc110-N, and CaMzt1 are all integral parts of the three-way interactions required for targeting Caγ-TuSC at SPBs in *C. albicans*.

Mzt1, the Spc98-N, and γ-TuCRs constitute the "oligomerization chaperone" module

In addition to targeting γ-tubulin complex to MTOCs, our study suggests that Mzt1 cooperates with γ-TuCRs to direct and promote γ-TuSC oligomerization into MT nucleation-competent rings (Fig. 8). Although CaMzt1 alone helped Caγ-TuSC overcome the low propensity for oligomerization, the resulting CaMzt1-Caγ-TuSC oligomers were not well organized and incompatible for MT nucleation. In contrast, the efficiency of CaSpc110-N alone in promoting Caγ-TuSC oligomerization is not as high as the case of *S. cerevisiae*, and the resulting Caγ-TuSC–CaSpc110-N assembly is also disorganized, failing to nucleate MTs. Only the combination of CaMzt1 and CaSpc110 yielded Caγ-TuSC oligomers with a diameter of 30 nm that were MT nucleation competent. We therefore propose that Mzt1 and γ-TuCRs cooperatively promote and

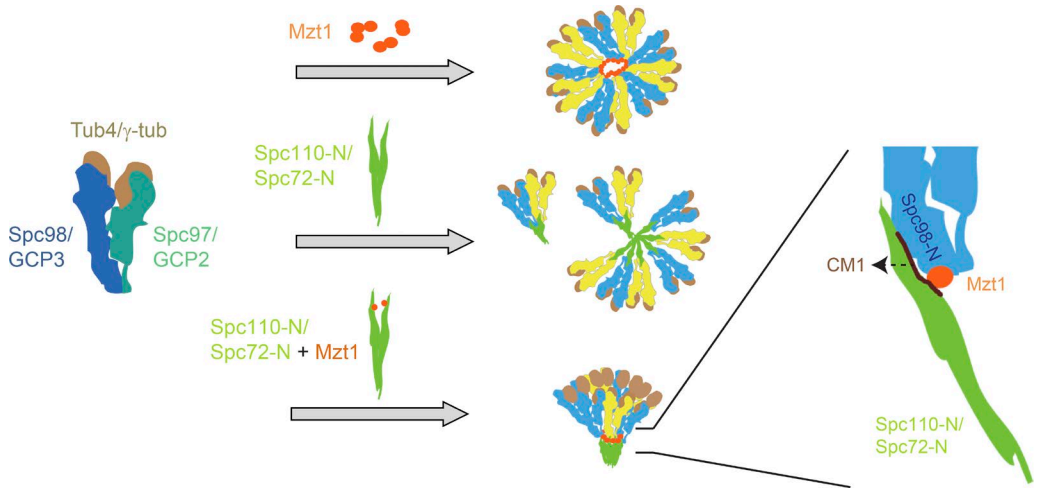

Figure 8. **Oligomerization chaperone model for MT nucleation template assembly.** See Discussion for details.

direct γ-TuSC oligomerization into well-organized and active MT nucleation template.

Such an additional role for MOZART1/Mzt1 on top of its function as a γ-tubulin complex targeting factor is conserved in human. siRNA depletion of MOZART1 in human cells, not only delocalizes the γ-TuRC from centrosomes (Hutchins et al., 2010), but also affects its integrity (Fig. 7 E). Presently, we do not know whether this occurs at the level of γ-TuRC stability or assembly. Taken this together, we propose that MOZART1/Mzt1, by binding to the N termini of a subset of GCP proteins and γ-TuCR, recruits γ-tubulin complexes to the centrosome and ensures the integrity of the γ-TuRC.

Coevolution of γ-TuSC and γ-TuCRs bypassed the requirement of Mzt1 in *S. cerevisiae*

By comparing the biochemical properties of components MT nucleation systems of *C. albicans* and *S. cerevisiae*, we revealed an interesting example of molecular coevolution that allows *S. cerevisiae* to bypass Mzt1 function. Scγ-TuSC has a higher propensity to promote oligomerization than Caγ-TuSC. This is, in part, attributed to the properties of ScSpc98-N. The oligomerization properties of Caγ-TuSC became more alike to those of Scγ-TuSC when the amino terminal domains were swapped in CaSpc98-N and ScSpc98-N (Fig. 4 C). The gain of oligomerization property of Scγ-TuSC may reflect an important prerequisite for the Mzt1-independent stimulation of γ-TuSC oligomerization. Intriguingly, *S. cerevisiae spc98ΔN* cells are viable with mild MT defects (Lin et al., 2014), suggesting without Spc98-N, ScSpc110 is still able to oligomerize Scγ-TuSC into active MT nucleator. Compared with CaSpc110-N–Caγ-TuSC interaction, the gain of higher affinity toward Scγ-TuSC by ScSpc110 may compensate for the function of Spc98-N. The ScSpc110-N may provide the interface that allows Scγ-TuSC interactions in the oligomer. Collectively, we propose that Spc98-N and Spc110-N have coevolved to bypass the loss of *MZT1* gene in *S. cerevisiae* and other Saccharomycetaceae species.

The presence and absence of *MZT1* in *C. albicans* and *S. cerevisiae* may reflect the difference in MT organization. Although in *S. cerevisiae*, MT bundles are exclusively attached to SPBs (Winey et al., 1995), randomly distributed free MTs are frequently observed in *C. albicans* (Barton and Gull, 1988; Finley and Berman, 2005; Fig. 1). Interphase MTs that are unattached to the SPB were also reported in *S. pombe* (Hagan and Hyams, 1988). The so-called "interphase MTOC" at the minus end of these MTs contains γ-tubulin and the CM1-containing Mto1 (Sawin et al., 2004). In addition, we also observed that the emergence of MT bundles from SPBs is cell-cycle regulated in *C. albicans*. Such regulation of MT nucleation activity at SPBs is more similar to *S. pombe* than to *S. cerevisiae*. Thus, it is tempting to speculate that in both *C. albicans* and *S. pombe* Mzt1 is required to temporally regulate the MT nucleation activity at SPBs and to stabilize the assembled γ-TuSC oligomers, protecting the minus-end of free MTs, whereas in *S. cerevisiae*, such free MTs and timely regulation are not demanded, and thus *MZT1* was lost from genome. EM tomography of MTs in *C. albicans* will be necessary to make direct comparison and reveal the differences in MT organization among these fungal species.

In summary, this study has unveiled the evolutionarily conserved functions of MOZART1/Mzt1 and interaction network in MT nucleation template assembly. In addition to acting as a clamp to target the γ-tubulin complex to centrosomes/SPBs, it acts, alongside γ-TuCRs, as an oligomerization chaperone to promote and direct the γ-TuSC oligomerization into an organized, active MT nucleation template.

Materials and methods

Plasmid construction

The plasmid collection used in this study is listed in Table S2. For the plasmids used for the overexpression of recombinant proteins in *E. coli*, BamHI-digested pET28b and pGEX-6p-1 were used as backbone vectors, and the corresponding ORFs were fused using a Gibson Assembly kit (New England Biolabs, Inc.). To get the full-length coding sequences of CaMzt1 (orf19.4418.1), CaSpc97 (orf19.708), CaSpc98 (orf19.2600), and CaTub4 (orf19.1238), multiple synthesized and codon-optimized DNA fragments were assembled and recombined into BamHI-digested pFastBac-HTA plasmid using a Gibson Assembly kit. Multiple-point mutations were introduced on the original wild-type constructs by PCR using primer pairs encompassing the mutation sites, and the resulting PCR products were encircled by a Gibson Assembly kit. The mutation sites were confirmed by sequencing.

Construction of *C. albicans* strains for phenotype analysis

The *C. albicans* strains used in this study are listed in Table S3. Standard methods were used for *C. albicans* cell culture, molecular, and genetic manipulations as described previously (Vernay et al., 2012; Xu et al., 2014). Dox-repressible *CaMZT1* strains were constructed as described previously (Nakayama et al., 2000). Δ/pTet-*CaMZT1* strain was constructed by replacing one copy of the respective ORF with deletion cassette with NAT1 marker using homologous recombination. A Tet-off promoter was then inserted 5′ of CaMZT1 by homologous recombination using pCAU98 plasmid (Nakayama et al., 2000) as a template and primers with sequences homologous to *CaMZT1* and the region before the start codon. Strains were verified by PCR of extracted genomic DNA (Lõoke et al., 2011) using primers covering part of the CaMZT1 and the cassette marker. To visualize the localization of and depletion of CaMzt1, the Δ/pTet-*CaMZT1-GFP* strain as well as *CaSPC97-GFP* and *CaSPC98-GFP* strains were generated by homologous recombination, using pFA-GFP-ARG4 as described previously (Gola et al., 2003).

To repress *CaMZT1* expression, Δ/pTet-*CaMZT1* strain was grown in YEPD with 20 µg/ml Dox overnight. The culture was then diluted into fresh media containing 20 µg/ml Dox and grown for 4 h to mid-log phase. To visualize genomic DNA, cells were fixed with 8% PFA and then stained with DAPI. For the hyphal induction experiment, overnight-grown strains were diluted into YEPD media and grown at 30°C for 4 h. The culture was then shifted to YEPD media containing 50% FCS at 37°C for 2 h (Bassilana et al., 2005). Cells were washed with PBS three times and then sonicated before inspection.

Images were collected on an inverted microscope (Axio Observer Z1; ZEISS) equipped with a 100× Plan-Neofluar DICIII oil objective lens (NA 1.3; ZEISS). Images were acquired with a monochrome camera (EMCCD iXON+897; Andor Technology) controlled with Metamorph 7.8 software (Molecular Devices). Image acquisition was performed along the z axis with a step of 0.3 µm. The acquired images were deconvolved with Huygens 15.1 (Scientific Volume Imaging).

Protein purification

Subunits of γ-TuSC variants were coexpressed with the baculovirus-insect cell expression system. Purification of γ-TuSC variants was performed as described previously (Gombos et al., 2013). For the full complex purification (Caγ-TuSC–CaMzt1–CaSpc110-N and Caγ-TuSC–CaMzt1–CaSpc110-N), subunits of Caγ-TuSC, *CaMZT1-3Flag*, and *GST-CaSPC110-N/GST-CaSPC72-N* were coexpressed with the baculovirus-insect cell expression system. Protein complexes were purified with Glutathione Sepharose 4B (GE Healthcare) as described (Vinh et al., 2002). The eluted proteins were subjected to gel filtration (Superdex 200 16/60; GE Healthcare) to remove glutathione and excess GST-CaSpc110-N/GST-CaSpc72-N. The protein peak of void volume was further analyzed with Superset PC 2.3/30.

For the in vitro reconstitution, *MZT1*, *SPC110-N*, and *SPC72-N* variants with an N-terminal GST tag were overexpressed in *E. coli* and purified with Glutathione Sepharose 4B as described (Vinh et al., 2002). Proteins were eluted with 5 mM glutathione, concentrated, and run over a Superose 6 column (GE Healthcare) equilibrated in HB100 to remove glutathione. For the purification of 6xHis-CaMzt1 and EGFP-CaMzt1, HB100 buffer supplemented with protease inhibitor cocktail (1x, 11 873 580 001; Roche) was used as lysis buffer, and the cleared lysates were loaded onto the Ni-NTA column (Protino Ni-NTA Agarose; MACHEREY-NAGEL). After a wash with lysis buffer of 10 times the column volume, proteins were eluted with 200 mM imidazole and further polished with gel filtration (Supderdex 75 10/300 for 6xHis-CaMzt1 and Superose 6 10/300 for EGFP-CaMzt1; GE Healthcare).

In vitro reconstitution of Caγ-TuSC–CaMzt1 complexes

Purified γ-TuSC was mixed with EGFP-CaMzt1, GST-CaMzt1, or 6xHis-CaMzt1 in 1:5 molar ratio (2.3:11.5) in HB100 (40 mM Hepes, pH 7.4, 1 mM $MgCl_2$, 1 mM EGTA, and 100 mM KCl) or BRB80 (80 mM Pipes, pH 6.8, 1 mM EGTA, and 1 mM $MgCl_2$) buffer with salt as indicated in figure legends. After incubating for 1 h at 4°C, the protein mixture was applied to a gel filtration column (Superose 6 PC 3.2/30; GE Healthcare). Elution profiles were recorded as absorbance at 280 nm. For each fraction, 20% of sample volume was analyzed by SDS-PAGE. Proteins were detected by Coomassie brilliant blue (CBB) staining or immunoblotting.

Mass spectrometry identification of phosphorylation sites

Phosphopeptides were identified according to Dephoure et al. (2008). In brief, SDS-PAGE–separated GST-CaSpc110-N was cut out and subjected to trypsin digestion. After digest, phosphopeptides were enriched by immobilized metal affinity chromatography, starting with 25 µl PHOS-Select beads (Sigma-Aldrich). Enriched phosphopeptides were eluted and desalted by C18 columns (StageTips; Thermo Fisher Scientific). Peptides were analyzed by liquid chromatography-tandem mass spectrometry (Orbitrap Elite; Thermo Fisher Scientific), and data were processed using Proteome Discoverer software (v1.4; Thermo Fisher Scientific). Phosphorylation site localization was performed on the Mascot results using phospho*RS*.

Binding affinity measurement by MST

MST assays were performed with a Monolith NT.115 instrument (NanoTemper Technologies). Each titration curve consisted of 16 points prepared from a serial dilution of analytes and a constant concentration of the fluorescein-labeled ligand. To measure the binding affinity between Caγ-TuSC and its interacting partners, purified Caγ-TuSC was fluorescently labeled using an amine-reactive protein labeling kit (GREEN-NHS; NanoTemper Technologies). Increasing concentrations (∼1 to ∼100,000 nM) of recombinant GST–CaSpc110-N, GST–CaSpc72-N, or 6xHis-CaMzt1 were titrated against 150 nM labeled Caγ-TuSC. To measure the binding affinity between CaMzt1 and the N-terminal fragments of γ-TuCRs, recombinant EGFP-CaMzt1 was constructed and purified as constant ligand at 250 or 150 nM. Experiments were performed in HB100 buffer supplemented with 0.05% (wt/vol) Tween-20. The samples were loaded into standard glass capillaries (Monolith NT capillaries; NanoTemper Technologies). MST assays were performed with 60 or 90% LED power using a green filter and a 40 or 60% MST power. The normalized fluorescence readings (thermophoresis plus T-jump) were plotted as a function of analyte concentration, and the curve fitting and dissociation constant K_d calculation were performed with NanoTemper software.

In vitro MT nucleation assay

MT nucleation assay was performed as described previously (Gombos et al., 2013) with some modifications. 1 µM Caγ-TuSC was preincubated with 13 µM GST–CaSpc110-N or 12.2 µM GST–CaSpc72-N and/or 14 µM GST-CaMzt1 in BRB80 containing 150 mM KCl, 12.5% glycerol (vol/vol), and 1 mM GTP for 30 min on ice. To overcome the suboptimal interspecies binding between tubulin and γ-tubulin, low concentrations of taxol (1 µM) were supplemented to stabilize MT seeds nucleated from Caγ-TuSC without inducing spontaneous MT polymerization (Fig. S5 D). Subsequently, an equal volume of BRB80 containing 150 mM KCl, 12.5% glycerol, and 20 µM porcine brain tubulin with 2% Alexa Fluor 568–labeled tubulin was added. Samples were further incubated for 10 min on ice before being transferred to 37°C for 10 min for MT polymerization. Samples were fixed with 10 times volume of 1% formaldehyde in BRB80 and incubated 5 min at

room temperature. Fixed reaction mixture was further diluted with 20 times volume of cold BRB80 buffer, and 50 µl diluted aliquot was sedimented onto poly-lysine–coated coverslips with an HB-4 rotor at 25,600 *g* for 1 h. Samples were post-fixed with precooled methanol, mounted on slides with CitiFluor mounting media, and imaged with a fluorescence microscope as described. Microtubules were counted in 20 random fields for each sample in each experiment.

To test the effect of taxol on MT nucleation (Fig. S5 D), experiment was performed with Scγ-TuSC and GST–ScSpc110-N. 3 µM Scγ-TuSC was preincubated with 15 µM GST–ScSpc110-N in BRB80, 12.5% glycerol (vol/vol), 1 mM GTP, and 2% DMSO (control for taxol) or 1 µM taxol for 30 min on ice. Subsequently, an equal volume of BRB80, 12.5% glycerol, and Alexa Fluor 568–labeled porcine tubulin mixture was added. After incubation on ice for 10 min, samples were transferred to 37°C for 10 min for MT polymerization. Samples were fixed with 10 times volume of 1% formaldehyde in BRB80 and incubated 5 min at room temperature. Fixed-reaction mixture was directly applied on glass slide and imaged with a fluorescence microscope. MT numbers were counted in eight random fields for each sample.

Negative staining of protein complexes and single-particle EM analysis

To visualize γ-TuSC monomers and oligomers, proteins were stained with uranyl acetate and analyzed by EM. In brief, we coated 300- or 400-mesh copper-palladium grids with a thin carbon layer (∼8 nm) on the copper side. To enhance the hydrophilic affinity of the carbon layer, grids were glow discharged for 30–45 s directly before the preparation started. The protein solution was incubated for 30 s on the carbon mesh grids at room temperature. For Ni-NTA Gold labeling, after removing the residual sample droplet, one drop of Ni-NTA Gold (1:100) was then applied and incubated for 1 min at room temperature. The grids were washed and incubated in 2% uranyl acetate for 4 min and blotted on Whatman Grade 50 paper.

The images were acquired on an electron microscope (Tecnai F20; Thermo Fisher Scientific) with a bottom-mounted 4K, high-sensitivity charge-coupled device camera (Eagle; Thermo Fisher Scientific) at a nominal magnification of 50,000, operating at 200 kV. Images were taken at −2–4 µm defocus. Single-particle boxing and image classification was performed using the EMAN2 and IMAGIC. Approximately 4,000 to 6,000 particles from the γ-TuSC variants were selected manually using Boxer. The representative micrographs and boxed particles are shown in Fig. S2. Subsequent image processing was performed in IMAGIC, following the program's standard procedures. Particles were band-pass filtered and normalized in their gray value distribution and mass centered. Alignment and iterative refinement of class averages followed the procedures described previously (Kornprobst et al., 2016).

Immunoprecipitation with anti-CEP215 antibody

HEK293T cells were transfected with plasmids for overexpression of MOZART1-EGFP or EGFP only. After 24 h, cells were harvested (confluency 80–0%) and lysed with lysis buffer (20 mM Tris-Cl, pH 7.5, 150 mM NaCl, 0.5% NP-40, and 0.5 mM EDTA). After clearing the lysates by centrifugation (4°C, 14,000 rpm), antibody against CEP215 (homemade, guinea pig, 1:100) was added into the supernatant and incubated at 4°C. After 1 h, Dynabeads Protein A (Thermo Fisher Scientific) was added for an additional 1 h. Beads were washed with lysis buffer three times, boiled with sample buffer, and then loaded for SDS-PAGE followed by Western blot. 1% of the lysate supernatant was loaded as input control.

Analysis of γ-TuRC stability in MOZART1-depleted U2OS cells by sucrose-gradient analysis

MOZART1-depleted U2OS cells were collected, washed with PBS, and suspended in lysis buffer (150 mM NaCl, 50 mM Hepes, pH 7.5, 2 mM EDTA, 1 mM DTT, and 0.5% Triton X-100, protease inhibitor cocktails; 1x, Roche) and 0.1 mM GTP. Mechanical cells lysis was performed by pipetting 10 times and then incubating on ice for 15 min. Cell lysates were cleared by centrifugation, and the supernatants were applied on top of sucrose gradient. Stepwise sucrose gradient was established with HB100 buffers with 1 mM EGTA, 1 mM $MgCl_2$, and 0.1 mM GTP containing 5, 13.75, 22.5, 31.25, and 40% sucrose. Ultracentrifugation was performed with rotor SW60 Ti, at 39,000 rpm for 3 h. Fractions were collected with fraction collector (Teledyne Isco) and analyzed with SDS-PAGE and Western blotting with anti–γ-tubulin (1:2,000 dilution, antibody against EYHAATRPDYISWGT QDK peptide of γ-tubulin).

In vivo MT nucleation assay in U2OS cells

The protocol was described as published (Choi et al., 2010). Cells were treated with one round of siRNA (siMOZART1: s54042, 20 nM; Ambion) for 72 h. siNSC (GE Healthcare) was applied in parallel. Knockdown efficiency was confirmed by Western blotting analysis using anti-MOZART1 (ab178359; Abcam) and anti–γ-tubulin antibodies. After the knockdown and 24 h of transfection for overexpression of GFP-CEP215^{CM1}, cells were placed on ice in the cold room for 1 h to depolymerize MTs. Microtubule regrowth was initiated at 37°C and proceeded for various time periods (0, 0.5, and 1 min). Cells were fixed for 10–15 min at room temperature with 4% PFA in PBS, 10 mM EGTA, 1 mM $MgCl_2$, and 0.5% Triton X-100 before immunostaining. The antibodies used were anti–α-tubulin (mouse; clone DM1A, 1:500; Sigma-Aldrich) and anti–PCNT (rabbit, 1:2,000; Abcam). Nuclear DNA was stained with Hoechst. Quantification was performed with maximum projected image of α-tubulin signals. A single boxed area (50 × 50 pixels) distant from centrosome (>5 µm) in selected cells was quantified.

Bioinformatic analysis

Protein sequences of Mzt1 and the CM1 element and their homologues in selected organisms were aligned with MAFFT algorithm built in Jalview software (Waterhouse et al., 2009; Katoh and Standley, 2013). The relative frequency of each amino acid in each position of Mzt1 and CM1 element was visualized using the WebLogo 3.0 (Crooks et al., 2004).

Statistical analysis

Statistical analysis of fluorescence intensities, immunoblotting intensities, and in vitro MT numbers was performed with Prism 6.1 (GraphPad Software). One-way analysis of variance with Tukey's multiple-comparisons test was used to compare samples and obtain adjusted P values. Student's *t* test was used to compare two samples. The number of repeated experiments and sample size are indicated in figure legends. No statistical method was used to predetermine sample size. The experiments were not randomized. The investigators were not blinded to allocation during the experiments and outcome assessment. In general, the data showed normal distribution.

Online supplemental material

Table S1 shows the summary of putative ORF γ-TuSC components, γ-TuCRs, and *MZT1* in selected fungal species. Tables S2 and S3 describe the plasmids and yeast strains used in this study, respectively. Fig. S1 shows Ca*MZT1* is most likely essential in *C. albicans* and required for γ-TuSC localization at SPBs and proper MT organization through cell cycle. Fig. S2 shows a single particle of Nanogold-labeled Caγ-TuSC and representative negative-stained EM micrographs of γ-TuSC variants. Fig. S3 shows CaMzt1 is in oligomeric forms and promotes Caγ-TuSC oligomerization by stably interacting with Caγ-TuSCs.

Fig. S4 shows the domain/motif organization of CaSpc110 and CaSpc72 and their sequence conservation. Phospho-mutations of CaSpc110-N do not have effect on the binding to CaMzt1. Fig. S5 shows the interaction among CaSpc72-N, Caγ-TuSC, and CaMzt1 with gel filtration and MST assay. The functional complementary test of chimeric mutant *spc98* and *spc110* in *S. cerevisiae* and Western blotting for the protein expression level and siRNA knockdown efficiency in U2OS cells are also shown. Videos 1 and 2 show the *C. albicans* cell cycle progression without and with Dox repression of Ca*MZT1* expression, respectively.

Acknowledgments

The authors thank Dr. M. Mayer for the use of the MST equipment and Dr. G. Butler for helping with Fig. S1 A and Table S1.

The work of E. Schiebel is supported by Deutsche Forschungsgemeinschaft Schi295/4-2. T.-c. Lin received a short-term European Molecular Biology Organization fellowship (EMBO ASTF 314-2015) for the analysis of Ca*MZT1* in the laboratory of R. Arkowitz, supported by the Centre National de la Recherche Scientifique, Agence Nationale de la Recherche (grants ANR-13-BSV3-0006-01 and ANR-11-LABX-0028-01), and Association pour la Recherche sur le Cancer (grant 20141201949). T. Chinen was supported by a Japan Society for the Promotion of Science Postdoctoral Fellowship for Research Abroad. P. Liu was awarded a Hartmut Hoffmann-Berling International Graduate School fellowship.

The authors declare no competing financial interests.

Submitted: 20 June 2016
Revised: 3 October 2016
Accepted: 4 November 2016

References

Anders, A., P.C. Lourenço, and K.E. Sawin. 2006. Noncore components of the fission yeast gamma-tubulin complex. *Mol. Biol. Cell.* 17:5075–5093. http://dx.doi.org/10.1091/mbc.E05-11-1009

Barton, R., and K. Gull. 1988. Variation in cytoplasmic microtubule organization and spindle length between the two forms of the dimorphic fungus *Candida albicans*. *J. Cell Sci.* 91:211–220.

Bassilana, M., J. Hopkins, and R.A. Arkowitz. 2005. Regulation of the Cdc42/Cdc24 GTPase module during *Candida albicans* hyphal growth. *Eukaryot. Cell.* 4:588–603. http://dx.doi.org/10.1128/EC.4.3.588-603.2005

Choi, Y.K., P. Liu, S.K. Sze, C. Dai, and R.Z. Qi. 2010. CDK5RAP2 stimulates microtubule nucleation by the γ-tubulin ring complex. *J. Cell Biol.* 191:1089–1095. http://dx.doi.org/10.1083/jcb.201007030

Choy, R.M., J.M. Kollman, A. Zelter, T.N. Davis, and D.A. Agard. 2009. Localization and orientation of the γ-tubulin small complex components using protein tags as labels for single particle EM. *J. Struct. Biol.* 168:571–574. http://dx.doi.org/10.1016/j.jsb.2009.08.012

Colombié, N., C. Vérollet, P. Sampaio, A. Moisand, C. Sunkel, H.M. Bourbon, M. Wright, and B. Raynaud-Messina. 2006. The *Drosophila* γ-tubulin small complex subunit Dgrip84 is required for structural and functional integrity of the spindle apparatus. *Mol. Biol. Cell.* 17:272–282. http://dx.doi.org/10.1091/mbc.E05-08-0722

Crooks, G.E., G. Hon, J.M. Chandonia, and S.E. Brenner. 2004. WebLogo: A sequence logo generator. *Genome Res.* 14:1188–1190. http://dx.doi.org/10.1101/gr.849004

Dephoure, N., C. Zhou, J. Villén, S.A. Beausoleil, C.E. Bakalarski, S.J. Elledge, and S.P. Gygi. 2008. A quantitative atlas of mitotic phosphorylation. *Proc. Natl. Acad. Sci. USA*. 105:10762–10767. http://dx.doi.org/10.1073/pnas.0805139105

Dhani, D.K., B.T. Goult, G.M. George, D.T. Rogerson, D.A. Bitton, C.J. Miller, J.W. Schwabe, and K. Tanaka. 2013. Mzt1/Tam4, a fission yeast MOZART1 homologue, is an essential component of the γ-tubulin complex and directly interacts with GCP3(Alp6). *Mol. Biol. Cell.* 24:3337–3349. http://dx.doi.org/10.1091/mbc.E13-05-0253

Finley, K.R., and J. Berman. 2005. Microtubules in *Candida albicans* hyphae drive nuclear dynamics and connect cell cycle progression to morphogenesis. *Eukaryot. Cell.* 4:1697–1711. http://dx.doi.org/10.1128/EC.4.10.1697-1711.2005

Gola, S., R. Martin, A. Walther, A. Dünkler, and J. Wendland. 2003. New modules for PCR-based gene targeting in *Candida albicans*: Rapid and efficient gene targeting using 100 bp of flanking homology region. *Yeast.* 20:1339–1347. http://dx.doi.org/10.1002/yea.1044

Gombos, L., A. Neuner, M. Berynskyy, L.L. Fava, R.C. Wade, C. Sachse, and E. Schiebel. 2013. GTP regulates the microtubule nucleation activity of γ-tubulin. *Nat. Cell Biol.* 15:1317–1327. http://dx.doi.org/10.1038/ncb2863

Gunawardane, R.N., O.C. Martin, K. Cao, L. Zhang, K. Dej, A. Iwamatsu, and Y. Zheng. 2000. Characterization and reconstitution of *Drosophila* γ-tubulin ring complex subunits. *J. Cell Biol.* 151:1513–1524. http://dx.doi.org/10.1083/jcb.151.7.1513

Hagan, I.M., and J.S. Hyams. 1988. The use of cell division cycle mutants to investigate the control of microtubule distribution in the fission yeast *Schizosaccharomyces pombe*. *J. Cell Sci.* 89:343–357.

Hutchins, J.R., Y. Toyoda, B. Hegemann, I. Poser, J.K. Hériché, M.M. Sykora, M. Augsburg, O. Hudecz, B.A. Buschhorn, J. Bulkescher, et al. 2010. Systematic analysis of human protein complexes identifies chromosome segregation proteins. *Science.* 328:593–599. http://dx.doi.org/10.1126/science.1181348

Janski, N., K. Masoud, M. Batzenschlager, E. Herzog, J.L. Evrard, G. Houlné, M. Bourge, M.E. Chabouté, and A.C. Schmit. 2012. The GCP3-interacting proteins GIP1 and GIP2 are required for γ-tubulin complex protein localization, spindle integrity, and chromosomal stability. *Plant Cell.* 24:1171–1187. http://dx.doi.org/10.1105/tpc.111.094904

Jerabek-Willemsen, M., C.J. Wienken, D. Braun, P. Baaske, and S. Duhr. 2011. Molecular interaction studies using microscale thermophoresis. *Assay Drug Dev. Technol.* 9:342–353. http://dx.doi.org/10.1089/adt.2011.0380

Katoh, K., and D.M. Standley. 2013. MAFFT multiple sequence alignment software version 7: Improvements in performance and usability. *Mol. Biol. Evol.* 30:772–780. http://dx.doi.org/10.1093/molbev/mst010

Knop, M., and E. Schiebel. 1997. Spc98p and Spc97p of the yeast γ-tubulin complex mediate binding to the spindle pole body via their interaction with Spc110p. *EMBO J.* 16:6985–6995. http://dx.doi.org/10.1093/emboj/16.23.6985

Knop, M., and E. Schiebel. 1998. Receptors determine the cellular localization of a γ-tubulin complex and thereby the site of microtubule formation. *EMBO J.* 17:3952–3967. http://dx.doi.org/10.1093/emboj/17.14.3952

Kollman, J.M., A. Zelter, E.G. Muller, B. Fox, L.M. Rice, T.N. Davis, and D.A. Agard. 2008. The structure of the γ-tubulin small complex: Implications of its architecture and flexibility for microtubule nucleation. *Mol. Biol. Cell.* 19:207–215. http://dx.doi.org/10.1091/mbc.E07-09-0879

Kollman, J.M., J.K. Polka, A. Zelter, T.N. Davis, and D.A. Agard. 2010. Microtubule nucleating gamma-TuSC assembles structures with 13-fold microtubule-like symmetry. *Nature.* 466:879–882. http://dx.doi.org/10.1038/nature09207

Kornprobst, M., M. Turk, N. Kellner, J. Cheng, D. Flemming, I. Koš-Braun, M. Koš, M. Thoms, O. Berninghausen, R. Beckmann, and E. Hurt. 2016. Architecture of the 90S pre-ribosome: A structural view on the birth of the eukaryotic ribosome. *Cell.* 166:380–393. http://dx.doi.org/10.1016/j.cell.2016.06.014

Lin, T.C., A. Neuner, Y.T. Schlosser, A.N. Scharf, L. Weber, and E. Schiebel. 2014. Cell-cycle dependent phosphorylation of yeast pericentrin regulates γ-TuSC-mediated microtubule nucleation. *eLife.* 3:e02208. http://dx.doi.org/10.7554/eLife.02208

Lin, T.C., A. Neuner, and E. Schiebel. 2015. Targeting of γ-tubulin complexes to microtubule organizing centers: conservation and divergence. *Trends Cell Biol.* 25:296–307. http://dx.doi.org/10.1016/j.tcb.2014.12.002

Liu, J., and C.A. Lessman. 2007. Soluble tubulin complexes, gamma-tubulin, and their changing distribution in the zebrafish (*Danio rerio*) ovary, oocyte and embryo. *Comp. Biochem. Physiol. B Biochem. Mol. Biol.* 147:56–73. http://dx.doi.org/10.1016/j.cbpb.2006.12.014

Lõoke, M., K. Kristjuhan, and A. Kristjuhan. 2011. Extraction of genomic DNA from yeasts for PCR-based applications. *Biotechniques.* 50:325–328. http://dx.doi.org/10.2144/000113672

Lyon, A.S., G. Morin, M. Moritz, K.C. Yabut, T. Vojnar, A. Zelter, E. Muller, T.N. Davis, and D.A. Agard. 2016. Higher-order oligomerization of Spc110p drives γ-tubulin ring complex assembly. *Mol. Biol. Cell.* 27:2245–2258. http://dx.doi.org/10.1091/mbc.E16-02-0072

Mackenzie, D.W. 1962. Serum tube identification of *Candida albicans*. *J. Clin. Pathol.* 15:563–565. http://dx.doi.org/10.1136/jcp.15.6.563

Martin, O.C., R.N. Gunawardane, A. Iwamatsu, and Y. Zheng. 1998. Xgrip109: A γ tubulin-associated protein with an essential role in gamma tubulin ring complex (γTuRC) assembly and centrosome function. *J. Cell Biol.* 141:675–687. http://dx.doi.org/10.1083/jcb.141.3.675

Masuda, H., and T. Toda. 2016. Synergistic role of fission yeast Alp16GCP6 and Mzt1MOZART1 in γ-tubulin complex recruitment to mitotic spindle pole bodies and spindle assembly. *Mol. Biol. Cell.* 27:1753–1763. http://dx.doi.org/10.1091/mbc.E15-08-0577

Masuda, H., R. Mori, M. Yukawa, and T. Toda. 2013. Fission yeast MOZART1/Mzt1 is an essential γ-tubulin complex component required for complex recruitment to the microtubule organizing center, but not its assembly. *Mol. Biol. Cell.* 24:2894–2906. http://dx.doi.org/10.1091/mbc.E13-05-0235

Muller, E.G., B.E. Snydsman, I. Novik, D.W. Hailey, D.R. Gestaut, C.A. Niemann, E.T. O'Toole, T.H. Giddings Jr., B.A. Sundin, and T.N. Davis. 2005. The organization of the core proteins of the yeast spindle pole body. *Mol. Biol. Cell.* 16:3341–3352. http://dx.doi.org/10.1091/mbc.E05-03-0214

Murphy, S.M., A.M. Preble, U.K. Patel, K.L. O'Connell, D.P. Dias, M. Moritz, D. Agard, J.T. Stults, and T. Stearns. 2001. GCP5 and GCP6: Two new members of the human gamma-tubulin complex. *Mol. Biol. Cell.* 12:3340–3352. http://dx.doi.org/10.1091/mbc.12.11.3340

Nakamura, M., and T. Hashimoto. 2009. A mutation in the Arabidopsis γ-tubulin-containing complex causes helical growth and abnormal microtubule branching. *J. Cell Sci.* 122:2208–2217. http://dx.doi.org/10.1242/jcs.044131

Nakamura, M., N. Yagi, T. Kato, S. Fujita, N. Kawashima, D.W. Ehrhardt, and T. Hashimoto. 2012. Arabidopsis GCP3-interacting protein 1/MOZART 1 is an integral component of the γ-tubulin-containing microtubule nucleating complex. *Plant J.* 71:216–225. http://dx.doi.org/10.1111/j.1365-313X.2012.04988.x

Nakayama, H., T. Mio, S. Nagahashi, M. Kokado, M. Arisawa, and Y. Aoki. 2000. Tetracycline-regulatable system to tightly control gene expression in the pathogenic fungus *Candida albicans*. *Infect. Immun.* 68:6712–6719. http://dx.doi.org/10.1128/IAI.68.12.6712-6719.2000

Samejima, I., V.J. Miller, L.M. Groocock, and K.E. Sawin. 2008. Two distinct regions of Mto1 are required for normal microtubule nucleation and efficient association with the γ-tubulin complex in vivo. *J. Cell Sci.* 121:3971–3980. http://dx.doi.org/10.1242/jcs.038414

Sawin, K.E., P.C. Lourenco, and H.A. Snaith. 2004. Microtubule nucleation at non-spindle pole body microtubule-organizing centers requires fission yeast centrosomin-related protein mod20p. *Curr. Biol.* 14:763–775. http://dx.doi.org/10.1016/j.cub.2004.03.042

Seltzer, V., N. Janski, J. Canaday, E. Herzog, M. Erhardt, J.L. Evrard, and A.C. Schmit. 2007. Arabidopsis GCP2 and GCP3 are part of a soluble gamma-tubulin complex and have nuclear envelope targeting domains. *Plant J.* 52:322–331. http://dx.doi.org/10.1111/j.1365-313X.2007.03240.x

Tange, Y., A. Fujita, T. Toda, and O. Niwa. 2004. Functional dissection of the gamma-tubulin complex by suppressor analysis of gtb1 and alp4 mutations in *Schizosaccharomyces pombe*. *Genetics.* 167:1095–1107. http://dx.doi.org/10.1534/genetics.104.027946

Teixidó-Travesa, N., J. Villén, C. Lacasa, M.T. Bertran, M. Archinti, S.P. Gygi, C. Caelles, J. Roig, and J. Lüders. 2010. The gammaTuRC revisited: A comparative analysis of interphase and mitotic human gammaTuRC redefines the set of core components and identifies the novel subunit GCP8. *Mol. Biol. Cell.* 21:3963–3972. http://dx.doi.org/10.1091/mbc.E10-05-0408

Vernay, A., S. Schaub, I. Guillas, M. Bassilana, and R.A. Arkowitz. 2012. A steep phosphoinositide bis-phosphate gradient forms during fungal filamentous growth. *J. Cell Biol.* 198:711–730. http://dx.doi.org/10.1083/jcb.201203099

Vinh, D.B.N., J.W. Kern, W.O. Hancock, J. Howard, and T.N. Davis. 2002. Reconstitution and characterization of budding yeast γ-tubulin complex. *Mol. Biol. Cell*. 13:1144–1157. http://dx.doi.org/10.1091/mbc.02-01-0607

Waterhouse, A.M., J.B. Procter, D.M. Martin, M. Clamp, and G.J. Barton. 2009. Jalview Version 2--a multiple sequence alignment editor and analysis workbench. *Bioinformatics.* 25:1189–1191. http://dx.doi.org/10.1093/bioinformatics/btp033

Winey, M., C.L. Mamay, E.T. O'Toole, D.N. Mastronarde, T.H. Giddings Jr., K.L. McDonald, and J.R. McIntosh. 1995. Three-dimensional ultrastructural analysis of the *Saccharomyces cerevisiae* mitotic spindle. *J. Cell Biol.* 129:1601–1615. http://dx.doi.org/10.1083/jcb.129.6.1601

Xiong, Y., and B.R. Oakley. 2009. In vivo analysis of the functions of γ-tubulin-complex proteins. *J. Cell Sci.* 122:4218–4227. http://dx.doi.org/10.1242/jcs.059196

Xu, Q.R., L. Yan, Q.Z. Lv, M. Zhou, X. Sui, Y.B. Cao, and Y.Y. Jiang. 2014. Molecular genetic techniques for gene manipulation in *Candida albicans*. *Virulence.* 5:507–520. http://dx.doi.org/10.4161/viru.28893

Zhang, L., T.J. Keating, A. Wilde, G.G. Borisy, and Y. Zheng. 2000. The role of Xgrip210 in γ-tubulin ring complex assembly and centrosome recruitment. *J. Cell Biol.* 151:1525–1536. http://dx.doi.org/10.1083/jcb.151.7.1525